Received: 1 December 2020 | Revised: 6 September 2021 | Accepted: 15 September 2021

DOI: 10.1111/bph.15693

RESEARCH ARTICLE

Butyrate ameliorates skeletal muscle atrophy in diabetic nephropathy by enhancing gut barrier function and FFA2-mediated PI3K/Akt/mTOR signals

Gang Tang | Yi Du | Haochen Guan | Jieshuang Jia | Nan Zhu | Yuping Shi | Shu Rong | Weijie Yuan

Department of Nephrology, Shanghai General Hospital, Shanghai Jiao Tong University School of Medicine, Shanghai, China

Correspondence
Weijie Yuan and Shu Rong, Department of Nephrology, Shanghai General Hospital, Shanghai Jiao Tong University School of Medicine, 100 Haining Road, Shanghai 200080, China.
Email: ywj4168@163.com; sophiars@126.com

Funding information
National Natural Science Foundation of China, Grant/Award Numbers: 81700621, 81970624

Background and Purpose: Muscle protein catabolism in patients with diabetic nephropathy (DN) results in striking loss of muscle proteins, which increases morbidity and mortality risks. Evidence shows that short-chain fatty acids (SCFAs) play an important role in health maintenance and disease development. Recently, the connection between butyrate (a SCFA) and DN has been revealed, although the relationship between butyrate and muscle atrophy remains unclear.

Experimental Approach: We studied changes in serum butyrate levels in DN patients using metabolomic analyses. In db/db mice, protective effects of butyrate on DN-induced muscle atrophy. were explored. Inhibition of muscle atrophy by butyrate and the underlying mechanism(s) were studied in C2C12 cells exposed to high glucose/lipopolysaccharide (HG/LPS).

Key Results: Butyrate levels in DN patients were significantly decreased. In db/db mice, supplementing normal diet with butyrate improved intestinal barrier function. Concurrently, butyrate alleviated muscle atrophy, promoted PI3K/Akt/mTOR signalling, and suppressed oxidative stress and autophagy in skeletal muscle of db/db mice, and in HG/LPS-exposed C2C12 cells. Further, FFA2 receptors, key components of SCFA signalling, were decreased in skeletal muscle of db/db mice and in HG/LPS-exposed C2C12 cells. Overexpression of FFA2 receptors activated PI3K/Akt/mTOR signalling and inhibited oxidative stress and autophagy in HG/LPS-exposed C2C12 cells. Silencing of FFA2 blocked PI3K/Akt/mTOR signalling that was improved by butyrate, as well as the suppression of oxidative stress and reduction of autophagy.

Conclusion and Implication: Butyrate exerts protective effects on muscle atrophy induced by DN by enhancing intestinal barrier function and activating the FFA2 receptor-mediated PI3K/Akt/mTOR pathway.

KEYWORDS
butyrate, db/db mice, diabetic nephropathy, FFA2, muscle atrophy

Abbreviations: BUN, blood urea nitrogen; CAT, catalase; CKD, chronic kidney disease; DN, diabetic nephropathy; ESRD, end-stage renal disease; GSH-Px, glutathione peroxidase; HG, high glucose; LPS, lipopolysaccharide; MDA, malondialdehyde; mTOR, mechanistic target of rapamycin kinase; ROS, reactive oxygen species; SCFAs, short-chain fatty acids; SOD, superoxide dismutase; TEM, transmission electron microscopy; UPS, ubiquitin-proteasome system.

Gang Tang, Yi Du, and Haochen Guan contributed equally to this work.

1 | INTRODUCTION

Protein-energy wasting is a state of disordered catabolism resulting from metabolic and nutritional derangements in chronic disease states. Patients with diabetic nephropathy (DN) and end-stage renal disease (ESRD) exhibit muscle atrophy that contributes to frailty and morbidity (Hanna et al., 2020; Obi et al., 2015). Preventing protein-energy wasting is the most pressing clinical concern in DN. Catabolic pathways that cause protein wasting include activation of the ubiquitin-proteasome system (UPS), caspase-3, lysosomes and myostatin, a negative regulator of skeletal muscle growth (Wang & Mitch, 2014). Muscle atrophy is a manifestation of protein-energy wasting. Recently, oxidative stress and autophagy were found to be strongly associated with muscle atrophy (Abrigo et al., 2018; Wang & Mitch, 2014). Mounting evidence has shown that the PI3K/Akt/mTOR pathway is a major factor mediating the regulation of muscle protein metabolism (Franke et al., 2003; Katso et al., 2001; Wang et al., 2009; Wang & Mitch, 2014).

Research has shown that short chain fatty acids (SCFAs) play important roles in health maintenance and disease development. SCFAs are a subset of fatty acids produced by the gut microbiota during the fermentation of partially and nondigestible polysaccharides (Tan et al., 2014). Butyrate is a SCFA and reportedly plays a protective role against diabetes and kidney disease (Andrade-Oliveira et al., 2015; Xu et al., 2018). Our previous study found that butyrate alleviated DN. Furthermore, we conducted both in vivo and in vitro experiments to shown that butyrate ameliorated renal fibrosis (Du et al., 2020).

Intestinal dysbiosis is a common phenomenon in DN. Uraemia significantly contributes to dysbiosis and alters the biochemical environment of the gut (Anders et al., 2013; Nallu et al., 2017; Vaziri et al., 2013). This can lead to alteration of tight junction (TJ) proteins in intestinal epithelial cells, which results in impairment of intestinal barrier function. In uraemic rats, the colonic epithelial TJ apparatus was disrupted (Vaziri et al., 2012). These events enable leakage of noxious contents, including phenols, cresols, and lipopolysaccharide (LPS), into the intestinal wall and systemic circulation (Nallu et al., 2017; Vaziri et al., 2016). The presence of various toxic biomolecules can also aggravate muscle atrophy, along with associated diseases, such as diabetes and DN. Disordered energy metabolism is a specific characteristic of DN. Mechanisms that may cause muscle atrophy in a rat model of CKD and db/db mice have been investigated (Kim et al., 2019; Wang et al., 2019). In the muscles of all models of diabetes or CKD, levels of mammalian target of rapamycin (mTOR) markers were decreased. Akt signalling and its downstream signalling are unique in that it controls both protein synthesis and protein degradation (Sandri, 2013). mTOR is at the centre of several cellular processes, such as downstream of Akt signalling. Thus, the development of a new compound specifically activating the Akt pathway may be extremely useful for counteracting muscle atrophy.

Another major mechanism resulting in muscle atrophy in DN is autophagy and lysosomal proteolysis. Importantly, the formation of autophagosomes is stimulated by decreased levels of PI3K. An increase in the levels of the PI3K/Akt signalling pathway is critical for autophagy suppression (Sandri, 2013; Wang & Mitch, 2014). Recent studies have demonstrated that oxidative stress can initiate autophagosome formation and autophagic degradation by acting as cellular signalling molecules (Glick et al., 2010). However, the effect of butyrate on these mechanisms and muscle atrophy remains to be established.

To explore the role of butyrate in muscle atrophy caused by DN, we first assessed the level of butyrate in the blood of DN patients and healthy people. In a model of diabetes, db/db mice, the effects of dietary supplementation with butyrate were compared with those of a normal diet. Urinary albumin, serum creatinine, blood urea nitrogen (BUN), and muscle weight were used as indicators of renal function and skeletal muscle atrophy, respectively. The levels of ZO-1, occludin, and mucin were determined to show changes in intestinal barrier function in db/db mice with or without butyrate supplementation. Malondialdehyde (MDA) and the activity of superoxide dismutase (SOD), catalase (CAT), and glutathione peroxidase (GSH-Px) were used to assess the oxidative stress state, while p62 and LC3-II were studied to explore the effect of butyrate on autophagy in skeletal muscle tissue in db/db mice and C2C12 myoblasts. The activation of the PI3K/Akt/mTOR pathway reflects the state of protein synthesis. To study the underlying mechanism by which butyrate ameliorates muscle atrophy, we focused on the free fatty acid receptor FFA2 (Milligan et al., 2009), the key molecule in signalling by SCFAs. Recently, SCFAs ameliorated DN by FFA2 receptor-mediated inhibition of oxidative stress (Huang et al., 2020) and SCFAs-treated diabetic mice were protected from nephropathy, but not in the absence of FFA2

What is already known

- Skeletal muscle atrophy is a pressing clinical concern in diabetic nephropathy, without effective therapeutic strategies.
- Butyrate is a short chain fatty acid which plays protective roles against many diseases.

What does this study add

- Serum butyrate levels were correlated with diabetic nephropathy and diabetic nephropathy-induced muscle atrophy.
- Butyrate ameliorates muscle atrophy via enhancing gut barrier function and FFA2 receptor-mediated PI3K/Akt/mTOR signalling.

What is the clinical significance

- Addition of butyrate provides a potentially effective strategy for treating diabetic nephropathy-induced muscle atrophy.

receptors (Li et al., 2020). Interestingly, although butyrate possessed beneficial effects on promoting glycogen metabolism in liver via FFA2 receptors in DN (Zhang et al., 2019), more recent studies confirmed that butyrate had no effect on blood glucose with or without FFA2 receptors (Huang et al., 2020; Li et al., 2020). Butyrate was also found to improve colonic epithelial barrier integrity by binding to FFA2 receptors (Cheng et al., 2018). In the present study, we have explored the therapeutic value of butyrate in DN-induced muscle atrophy.

2 | METHODS

2.1 | Human studies

The study was approved by the ethics committee of Shanghai General Hospital (2019KY014). All donors provided full informed consent. The clinical variables of the donors are shown in Table 1. All patients received insulin and there were almost no special co-morbidities for each patient.

Blood samples (5ml per sample. venous blood) were obtained from 15 in-patients and 42 healthy people at the Department of Nephrology and Physical Center, Shanghai General Hospital, Shanghai Jiao Tong University School of Medicine. ll in-patients were diagnosed with Type 2 diabetic nephropathy (DN) and nine of them were diagnosed with DN-induced protein-energy wasting, by at least three experienced nephrologists, based on the criteria proposed by the Joint Committee of Diabetic Nephropathy and the International Society of Renal Nutrition and Metabolism (ISRNM) (Fouque et al., 2008; Haneda et al., 2015). The criteria for DN were: Type 2 diabetic patients with urinary albumin excretion (UAE) >20 μg min^{-1} and ≤199 μg min^{-1} and for protein-energy wasting: serum albumin < 3.8 g per 100 ml; BMI<23; reduced muscle mass 5% over 3 months or 10% over 6 months; unintentional low dietary protein intake <0.80 g kg^{-1} day^{-1} for at least 2 months. All healthy subjects (NC group; Table 1) came from the medical center and had no criteria of DN or protein-energy wasting. None of the NC group were receiving prescription medicines or were self-medicating. Receiver operating characteristic (ROC) analysis was used to assess the diagnostic ability of a binary classifier system as its discrimination threshold is varied; in this case to calculate the cut-off value of butyrate level. We constructed a ROC curve and calculated the AUC to evaluate the accuracy for butyrate in the diagnosis of DN-induced protein-energy wasting.

2.2 | Blood sample preparation

Serum was obtained after centrifugation of whole blood and samples stored at -80°C for no more than 7 days before analysis. Samples were thawed in an ice-bath to minimize sample degradation. Serum (25 μl per well) was added to a 96-well plate. Then the plate was transferred to the Eppendorf epMotion Workstation (Eppendorf Inc., Hamburg, Germany). Ice cold methanol (120 μl) with partial internal standards was automatically added to each sample and vortexed vigorously for 5 min. The plate was centrifuged at 4000 × *g* for 30 min (Allegra X-15R, Beckman Coulter, Inc., Indianapolis, IN, USA). Then, the plate was returned to the workstation. Supernatant (30 μl) was transferred to a clean 96-well plate, and freshly prepared derivative reagents (20 μl) were added to each well. The plate was sealed, and the derivatization was carried out at 30°C for 60 min. After derivatization, 330-μl ice-cold 50% methanol solution was added to dilute the sample. The plate was then stored at −20°C for 20 min and centrifuged at 4000 × *g* at 4°C for 30 min; 135-μl supernatant was transferred to a new 96-well plate with 10-μl internal standards in each well. Serial dilutions of the derivatized stock standards were added to the remaining wells. Finally, the plate was sealed for liquid chromatography–mass spectrometry (LC-MS) analysis.

2.3 | Metabolomics analysis

Metabolomics analysis was performed using the Q300 Kit (Metabo-Profile, Shanghai, China). An ultraperformance liquid chromatography coupled to tandem mass spectrometry (UPLC-MS/MS) system (ACQUITY UPLC-Xevo TQ-S, Waters Corp., Milford, MA, USA) was used to quantitate all targeted metabolites in this study (Metabo-Profile Biotechnology [Shanghai] Co., Ltd). The optimized instrument settings are briefly described as follows. For HPLC, column: ACQUITY HPLC BEH C18 1.7 × 10–6 m VanGuard precolumn (2.1 × 5 mm) and ACQUITY HPLC BEH C18 1.7 × 10–6 m analytical column (2.1 × 100 mm), column temp.: 40°C, sample manager temp.: 10°C, mobile phases: A = water with 0.1% formic acid; and B = acetonitrile/IPA (70:30), gradient conditions: 0–1 min (5% B), 1–11 min (5%–78% B), 11–13.5 min (78%–95% B), 13.5–14 min (95%–100% B), 14–16 min (100% B), 16–16.1 min (100–5%B), 16.1–18 min (5% B), flow rate: 0.40 ml·min^{-1}, and injection volume: 5.0 μl. For the mass spectrometer, capillary: 1.5 (ESI+), 2.0 (ESI-) Kv, source temperature: 150°C, desolvation temperature: 550°C, and desolvation gas flow: 1000 L·h^{-1}.

For data processing, the raw data files generated by UPLC-MS/MS were processed using the iMAP platform (v1.0; Metabo-Profile, Shanghai, China) to calculate the concentration of each analyte in the samples. Principal component analysis (PCA) and orthogonal partial least squares discriminant analysis (OPLS-DA) were also performed with iMAP (v1.0). VIP Variable importance in projection (VIP) was obtained based on the OPLS-DA model. Metabolites with VIP ≥ 1 and *P* value <0.05 (univariate analyses were based on whether the data were normally distributed) were regarded as statistically significant (differentially expressed metabolites: DEMs). The *Z* score indicates how many standard deviations an observation is above or below the mean of the control group. The Vplot that integrates the fold change and *P* values was used to show the significantly different metabolites.

2.4 | Animals

All animal care and experimental procedures were approved by the Institutional Animal Care and Use Committee (IACUC) of Shanghai

General Hospital (2019DW001). All experimental design and analysis involving animals, animal tissues, or primary cultures were performed in compliance with the ARRIVE guidelines (Percie du Sert et al., 2020) and with the recommendations made by the British Journal of Pharmacology (Lilley et al., 2020).

Male db/db and db/m mice, 4 weeks old, were purchased from the Nanjing Institute of Model Animals. All mice were kept at the animal centre of the Shanghai General Hospital at 22°C under a 12-h light/12-h dark cycle with free access to water in individually ventilated cages with same size and wood shavings as bedding material (five to six mice per cage). When the mice were 8 weeks old, their blood glucose levels were randomly measured, and those with ≥16.7 mM of blood glucose were considered to be diabetic; 45 mice were marked with an earmark and allocated to nine groups (normal control [NC], DN model, DN + butyrate (DN + Bu), DN + TUG, DN + Bu + Alcohol, LV-CMV, DN + LV-CMV, DN + Bu + LV-CMV, DN + Bu + LV-FFA2) in a completely randomized manner using a randomized table ($n = 5$ per group).

A standard diet was administered to the mice in the NC and DN groups while those of the DN + Bu group were fed with a butyrate diet. This diet was prepared by blending the powdered form of butyrate (Sigma-Aldrich, MO, USA) with the standard diet using a food processor, followed by centrifugation at 18 × *g*, such that the final proportion of butyrate in the diet was 1% (Medicine, Nanjing, China). The diet containing butyrate was pelleted and stored in a freezer at −20°C until use. As in our previous studies (Du et al., 2020), mice fed the butyrate diet received 1 $g \cdot kg^{-1} \cdot day^{-1}$ of butyrate at the normal rate of caloric intake for a total period of 12 weeks (Dong et al., 2017). Their blood glucose and LPS levels were recorded on Mondays 4, 8, 12, 16, and 20 weeks after birth. We assayed the samples for glucose immediately after taking the blood using a Blood Glucose Test Meter and the LPS content of all samples was assayed after storing at -80°C, by a fully automated biochemical analyser (Rayto, Shenzhen, China). Urine was collected on the Monday morning of week 20 and urinary albumin, serum creatinine and BUN were detected using a fully automated biochemical analyser (Rayto, Shenzhen, China). Butyrate levels were also determined, using Gas chromatography-mass spectrometry (GC/MS). Mice were anaesthetized with isoflurane and asphyxiated with CO_2 at 20 weeks. The hindlimb and gastrocnemius muscles and serum were collected.

2.5 | Cell culture

C2C12 murine myoblast cells (KCB Cat# KCB 2012115YJ, RRID: CVCL_0188) were cultured in high-glucose Dulbecco's modified Eagle's medium (DMEM; Gibco, New York, USA) supplemented with 10% foetal bovine serum (FBS; Gibco, New York, USA), 2-mmol L-glutamine, and 1% penicillin–streptomycin (PS) solution (NCM biotech, Suzhou, China) in a humidified atmosphere containing 5% CO_2/95% air at 37°C. Cells were grown to confluence (approximately 6 days), at which point the medium was changed to differentiation media (DM) composed of DMEM plus 2% horse serum (HS) (HyClone, New York, USA), and 1% PS solution to initiate differentiation. LPS (Serotype: 0111:B4, Sigma-Aldrich, Munich, Germany) was used to induce oxidative stress and atrophy models in C2C12 myoblasts (Baker et al., 2018). After differentiation for 6 days, myotubes were exposed to one of three conditions (for 24 h): (i) negative control (NC): DM; (ii) high glucose/LPS (HG/LPS): DM + 30 $mM \cdot L^{-1}$ of glucose + 100 $ng \cdot ml^{-1}$ LPS; (iii) butyrate (HG/LPS + Bu): DM + 30 $mM \cdot L^{-1}$ of glucose + 100 $ng \cdot ml^{-1}$ LPS + 0.5-mM butyrate.

2.6 | Tissue processing

The colon and ileum were isolated at necropsy and stored at −80°C. The first one third of the ascending colon was cut for histology, and the next two thirds was cut and stored at −80°C for other studies. The gastrocnemius (1/4), isolated from the mice post-mortem, was fixed in 4% paraformaldehyde, embedded in paraffin, and cut into 5-μm thick sections. The remaining gastrocnemius was stored at −80°C for follow-up studies.

2.7 | RT-qPCR

TRIzol reagent (Cat# 15596-026, Invitrogen, CA, USA) was used to isolate total RNA, and RT-qPCR was performed using the TB Green™ Premix Ex Taq kits (Cat# RR420B, Takara, Shiga, Japan), according to the manufacturer's instructions. Primer sequences were checked for specificity and assay efficiency by performing standard curve analysis, and the sequences were as follows: IL-6, F: 5′-CTCCCAACAGACCTGTCTATAC-3′, R: 5′-CCATTGCACAACTCTTTTCTCA-3′; TNF-α, F: 5′-ATGTCTCAGCCTCTTCTCATTC-3′, R: 5′-GCTTGTCACTCGAATTTTGAGA-3′; IL-1β, F: 5′-TGATGAAAGACGGCACACCC-3′, R: 5′-TGTCCCGACCATTGCTGTTT-3′; CRP, F: 5′-CCTTCGTATTTCCCGGAGTGTC-3′, R: 5′-CTCACATCAGCGTGGGCATAG-3′; GAPDH, F: 5′-CTGGAGAAACCTGCCAAGTATG-3′, R: 5′-GGTGGAAGAATGGGAGTTGCT-3′.

2.8 | Enzyme-linked immunosorbent assay

Serum levels of IL-6, TNFα, IL-1β, and CRP were determined using IL-6 Quantikine ELISA Kit (R&D Cat# M6000B, RRID:AB_2877063), TNF-alpha Quantikine ELISA Kit (R&D Cat# MTA00B, RRID: AB_2877064), IL-1 beta/IL-1F2 Quantikine ELISA Kit (R&D Cat# MLB00C), and C-Reactive Protein/CRP Quantikine ELISA Kit (R&D Cat# MCRP00).

2.9 | Staining of muscle sections

After tissue processing, paraffin-embedded gastrocnemius sections were deparaffinized with xylene, washed with ethanol and then washed with water, and stained with haematoxylin and eosin (HE). Then, six images were taken randomly for each sample, and the

myofibre cross-sectional area of these images was analysed using Image J (ImageJ, RRID:SCR_003070).

2.10 | Transmission electron microscopy

The fresh gastrocnemius muscle was sectioned in 40-mm^3 blocks, immersed in fixative solution (0.5% glutaraldehyde, 2% paraformaldehyde, 7% saccharose, and 4% polyvinylpyrrolidone in 0.1-M cacodylate buffer) for 1 h, and rinsed with phosphate-buffered saline (PBS). These muscle blocks were recut into smaller samples of about 10 mm^3 and fixed with another fixative solution (2% osmic acid in 0.1-M cacodylate buffer) for 1 h. Subsequently, the samples were dehydrated, infiltrated, and embedded in Epon 812 at 60° for 48 h and cut into 0.1-μm thick longitudinal or transverse sections. These sections were stained with 1% uranyl acetate and Reynolds's lead citrate. They were observed under a Leica UC7 HT7700 (HITACHI) microscope to analyse the ultrastructure of mitochondria.

2.11 | Immunohistochemistry

The colon, ileum, and muscle tissue sections were subjected to heat treatment in a citrate solution for antigen clearance and incubated with 3% bovine serum albumin (BSA) blocking solution at room temperature for 30 min. Thereafter, the sections were incubated at 4°C overnight with corresponding primary antibodies (for colon and ileum: ZO-1, Abcam Cat# ab96587, RRID:AB_10680012 and Occludin, Santa Cruz Biotechnology Cat# sc-133256, RRID:AB_2156317, all 1:200. For muscle: FFA2, Bioss Cat# bs-13536R, 1:300). After incubation with goat anti-rabbit secondary antibody (1:200, Servicebio, Wuhan, China) at room temperature for 1 h, the slides were treated with DAB using Dako REAL Envision (K5007; Dako; Agilent Technologies, Inc.), according to the manufacturer's instructions.

2.12 | Immunofluorescence

Immunofluorescence (IF) staining was conducted as we previously described (Du et al., 2020). Briefly, tissue sections were incubated with corresponding primary antibodies (for colon and ileum: Muc2, Santa Cruz Biotechnology Cat# sc-7314, RRID:AB_627970, 1:100) at 4°C overnight, followed by incubation with corresponding anti-mouse secondary antibodies for 1 h at room temperature.

Regarding cells, C2C12 myoblasts grown on a four-chamber glass bottom dish (#D35C4-20-1-N; Cellvis, CA, USA) were fixed with 4% formaldehyde solution for 20 min. After washing with PBS twice, the cells were permeabilized with 0.2% Triton X-100 in PBS for 10 min, washed with PBS twice, and incubated with phalloidin (1:200 in PBS) to visualize the F-actin filaments in myotubes.

For tissue sections and cells, nuclei were stained with Antifade Mounting Medium with 4′,6-diamidino-2-phenylindole (DAPI) for 5 min.

2.13 | Alcian blue stain

Alcian blue staining is widely used for mucins (Kameyama et al., 2015). After dewaxing and hydration, the colon sections were exposed to Alcian blue stain for 30 min at room temperature. The sections were then dehydrated and mounted.

2.14 | Oxidative stress markers

Gastrocnemius (100 mg) preserved at −80°C was treated via ultrasonic grinding and centrifuged at 16972x*g* for 15 min at 4°C to obtain supernatants. Blood was centrifuged at 4481x*g* for 20 min to obtain serum. The activities of SOD, CAT, GSH-Px, and MDA were determined using detection kits (SOD: A001-3-2; CAT: A007-1; GSH-Px: A005-1-2; MDA: A003-1, Nanjing Jiancheng Bioengineering Institute Co., Ltd.) according to the manufacturer's protocols.

2.15 | ROS measurements

The intracellular levels of ROS were measured using a Reactive Oxygen Species Assay Kit (Cat# S0033S, Beyotime Biotechnology, China); 2′, 7′-dichlorofluorescein-diacetate (DCFH-DA), which is easily oxidized to fluorescent dichlorofluorescein (DCF) by intracellular ROS, is its principal component and therefore, its levels reflect those of ROS. Briefly, the cells were seeded in six-well plates as described above, and after 6 days of differentiation, myotubes were exposed to corresponding conditions. Following the treatment, the cells were incubated with DCFH-DA for 20 min at 37°C and then observed using a fluorescence microscope (Leica) and measured at 488 nm excitation and 525 nm emission by a fluorescence spectrophotometer (BioTek).

2.16 | Western blot

The tissues and cell samples were mixed with radioimmunoprecipitation assay (RIPA) lysis buffer containing phenyl methane sulfonyl fluoride (PMSF) and phosphatase inhibitors to isolate proteins. The samples were then centrifuged at 16972x*g* for 15 min, and the supernatant was collected for protein quantitation using a bicinchoninic acid (BCA) assay. Processed proteins were separated by sodium dodecyl sulphate polyacrylamide gel electrophoresis (SDS-PAGE) and transferred onto polyvinylidene difluoride (PVDF) membranes. After blocking with 5% skim milk for 1 h, the membranes were incubated overnight at 4°C with the following primary antibodies: ZO-1 (Abcam Cat# ab96587, RRID:AB_10680012), occluding (Santa Cruz Biotechnology Cat# sc-133256, RRID:AB_2156317), PI3K (Cell Signaling Technology Cat# 4257, RRID:AB_659889), p-PI3K (Cell Signaling Technology Cat# 4228, RRID:AB_659940), Akt (Cell Signaling Technology Cat# 4691, RRID:AB_915783), p-Akt (Cell Signaling

Technology Cat# 5012, RRID:AB_2224726), mTOR (Cell Signaling Technology Cat# 2983, RRID:AB_2105622), p-mTOR (Cell Signaling Technology Cat# 5536, RRID:AB_10691552), p62 (Cell Signaling Technology Cat# 23214, RRID:AB_2798858), LC3 II (Cell Signaling Technology Cat# 3868, RRID:AB_2137707), FFA2 (Bioss Cat# bs-13536R) (all 1:500); GAPDH (Cell Signaling Technology Cat# 5174, RRID:AB_10622025, 1:1000), and α-tubulin (Proteintech Cat# 11224-1-AP, RRID:AB_2210206, 1:1000). The membranes were then incubated with goat anti-rabbit (Absin Bioscience Cat# abs20002A, RRID:AB_2716554, 1:10000) or goat anti-mouse secondary antibodies (Absin Cat# abs20001, RRID:AB_2716555, 1:10000). Band visualization was performed using an electrochemiluminescence (ECL) reagent (NCM biotech, China). The blots were quantified using ImageJ software.

2.17 | Construction of stabilized FFA2 overexpression C2C12 myoblasts

FFA2 cDNA was amplified using PCR and cloned into the pGMLV-EF1 lentiviral vector (Genomeditech Inc., China). Stable cell lines that expressed FFA2 were selected by two rounds of treatment with 1.5 $\mu g \cdot ml^{-1}$ puromycin for 2 days. We constructed stable FFA2-overexpressing cell lines C2C12-FFA2 and their corresponding stable control cell lines C2C12-pGMLV vector.

2.18 | siRNA-mediated gene silencing of FFA2

To silence the FFA2 gene, we used a small interfering RNA (siRNA) that targets FFA2 (Genomeditech Inc., China) and the siRNA negative control, which does not target any known sequence. Transfection with 20-nM siRNA duplex was performed using Lipofectamine 3000 reagent (Cat# L3000015, Invitrogen, Life technologies, USA) according to the manufacturer's protocols. Cells were transfected for 48 h and then stimulated with 30 mM of glucose + 100 $ng \cdot ml^{-1}$ LPS in the presence or absence of 0.5-mM butyrate for 24 h.

2.19 | Data and statistical analysis

Statistical analysis was performed for studies with five independent values ($n = 5$). All data are presented as mean ± SD. The distribution of data was assessed by Kolmogorov–Smirnov test at first. If data followed a Gaussian distribution, parametric tests (Student's *t* test for two groups, or one-way ANOVA for three or more groups) were carried out; for ANOVA, Bonferroni's post hoc test was performed for data with *F* at $P < 0.05$ and no significant variance inhomogeneity. If data were not normally distributed, non-parametric tests (Mann–Whitney test for two groups or Kruskal–Wallis test with Dunn's post-test for three or more groups) were used by GraphPad Prism version 7.00 for Windows (GraphPad Software, RRID:SCR_002798) and SPSS Statistics 22 (IBM Corp., RRID:SCR_002865). A *P* value <0.05 was considered statistically significant. Blinding or randomization was carried out in all the experiments.

2.20 | Materials

FFA2 receptor agonist TUG-1375 (#HY-112813) and PI3K/Akt/mTOR pathway inhibitor PI3K-IN-1 (#HY-12068) were purchased from MedChemExpress (MCE, China).

2.21 | Nomenclature of targets and ligands

Key protein targets and ligands in this article are hyperlinked to corresponding entries in the IUPHAR/BPS Guide to PHARMACOLOGY (http://www.guidetopharmacology.org) and are permanently archived in the Concise Guide to PHARMACOLOGY 2021/22 (Alexander, Christopoulos, et al., 2021; Alexander, Fabbro, et al., 2021a, 2021b)

3 | RESULTS

3.1 | Serum butyrate levels are significantly correlated with DN and DN-induced muscle atrophy

To investigate the butyrate levels of patients with DN, targeted metabolomics analyses based on UPLC/MS were applied to investigate serum samples of 15 in-patients, and 42 healthy subjects. A total of 146 metabolites were identified in serum, 44 metabolites (38 potential biomarkers) were significantly up-regulated, 32 metabolites (nine potential biomarkers) were down-regulated, and 70 metabolites exhibited no change in DN serum (Figure 1a,b). The enrichment analysis found that the butyrate metabolism pathway was the most valuable metabolism pathway for further assessments (Figure 1c). Metabolomics analyses showed that serum butyrate levels decreased significantly in DN, compared with those in healthy subjects (Figure 2a). The ROC curve was plotted to evaluate the diagnostic value of muscle atrophy. The area under the ROC curve (AUC) was 0.815, suggesting a modest accuracy for butyrate in the diagnosis of muscle atrophy (Figure 2b).

In db/db mice, serum butyrate levels were lower than those of the NC group, while the diet containing butyrate contributed to a significant improvement in serum butyrate levels (Figure 2c). To evaluate the effect of butyrate on renal function, we investigated several biochemical criteria and found that the levels of serum creatinine, BUN, and the urinary albumin/creatinine ratio were within normal ranges in the NC group, while they were increased in the db/db mice. After supplementation with butyrate, significant reductions in the levels of serum creatinine, BUN, and the urinary albumin/creatinine ratio were observed in the butyrate group (Figure 2d–f). However, no obvious differences were observed in blood glucose levels when db/db mice received dietary butyrate supplementation (Figure 2g).

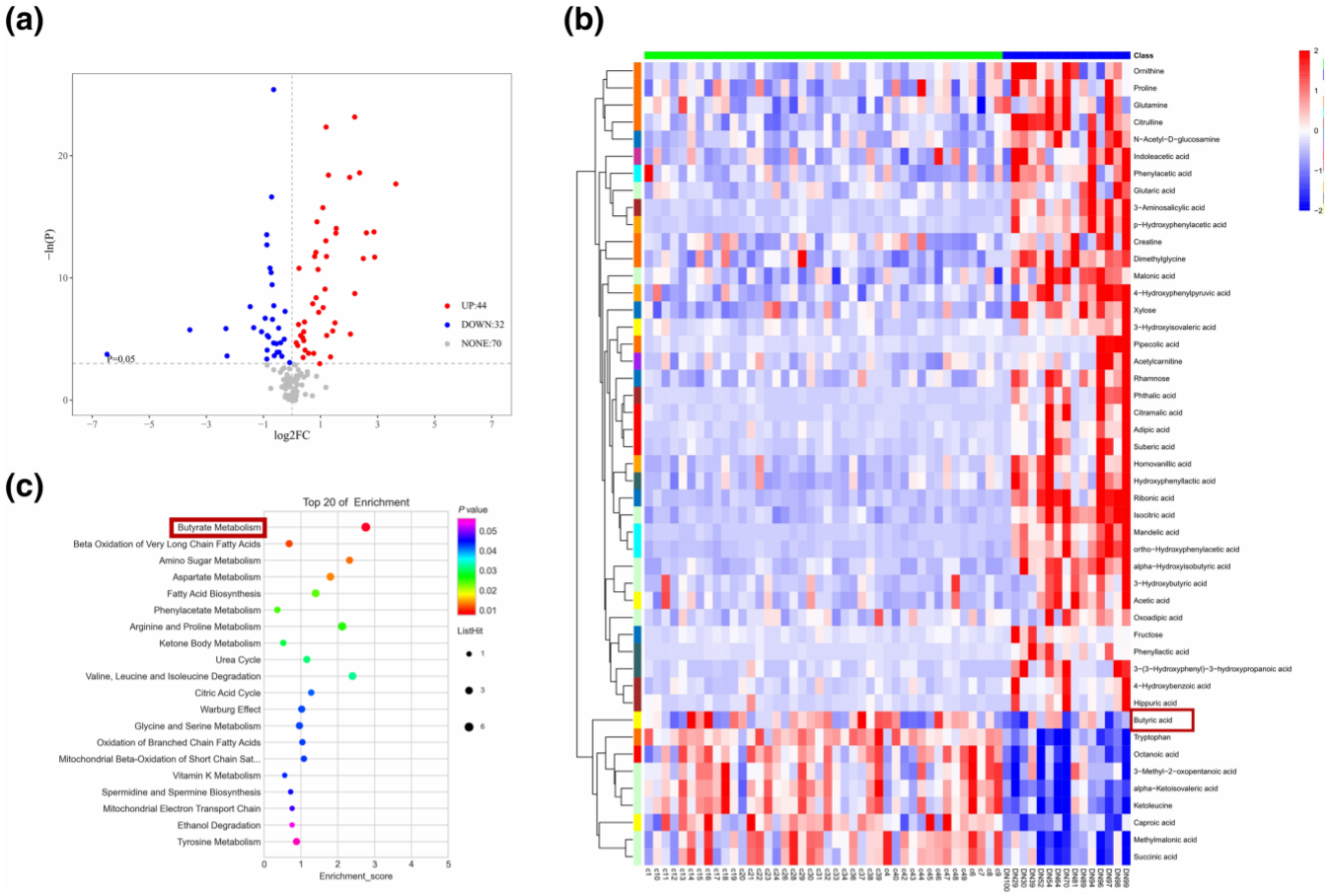

FIGURE 1 Metabolomics analysis. Metabolomics analysis found 146 metabolites in serum of DN patients and healthy people, according to the volcano plot (a). The metabolites of potential biomarkers with significant up-regulation (38) and down-regulation (9) metabolites are shown in the heatmap (b). Enrichment analysis for potential pathway is shown (c)

3.2 | Butyrate alleviated inflammation and reduced LPS levels in db/db mice

Circulating inflammation levels generally increased in patients with DN, and high levels of CRP predicted all-cause mortality, especially in patients with hypoalbuminemia. Levels of muscle and circulating pro-inflammatory cytokines, including **IL-6**, **TNFα**, **IL-1β** and CRP, were assayed in this study. In db/db mice, all proinflammatory cytokines increased significantly compared with those in the NC group. However, the levels of IL-6, TNFα, IL-1β, and CRP were markedly decreased after administration of the butyrate diet (Figure S1A–H). Conversely, serum LPS levels were significantly higher in db/db mice than in the NC group, and supplementation with butyrate inhibited this increase (Figure S1I,J).

3.3 | Butyrate ameliorated skeletal muscle atrophy

To observe the muscle alteration in different groups, we measured the hindlimb and gastrocnemius muscle mass of mice for comparison. The results showed that hindlimb and gastrocnemius muscle mass were significantly reduced in db/db mice compared with the NC group, while butyrate treatment blocked this decrease (Figure 3a–d). In the micro measurement, haematoxylin-eosin (HE) staining also showed that the cross-sectional area of muscle fibres in db/db mice was significantly smaller than that in the NC group, while butyrate treatment alleviated the atrophy (Figure 3e,f). In addition, myotubes incubated with HG/LPS for 48 h displayed an obvious level of morphological atrophy, with a nearly 50% reduction in myotube diameter, but no change in myotube number (Figure 3g–i). Butyrate treatment, along with HG/LPS, markedly prevented HG/LPS-induced atrophy, with no difference in myotube number.

3.4 | Butyrate enhanced gut barrier function

To explore the alterations in DN, we stained the ileum and colon with Alcian blue (Figure 4a,b), a dye known to stain mucin. Mucin expression in the db/db mice was significantly lower than that in the NC group. After butyrate treatment, mucin synthesis increased and mucin expression was elevated in all ileum and colon samples.

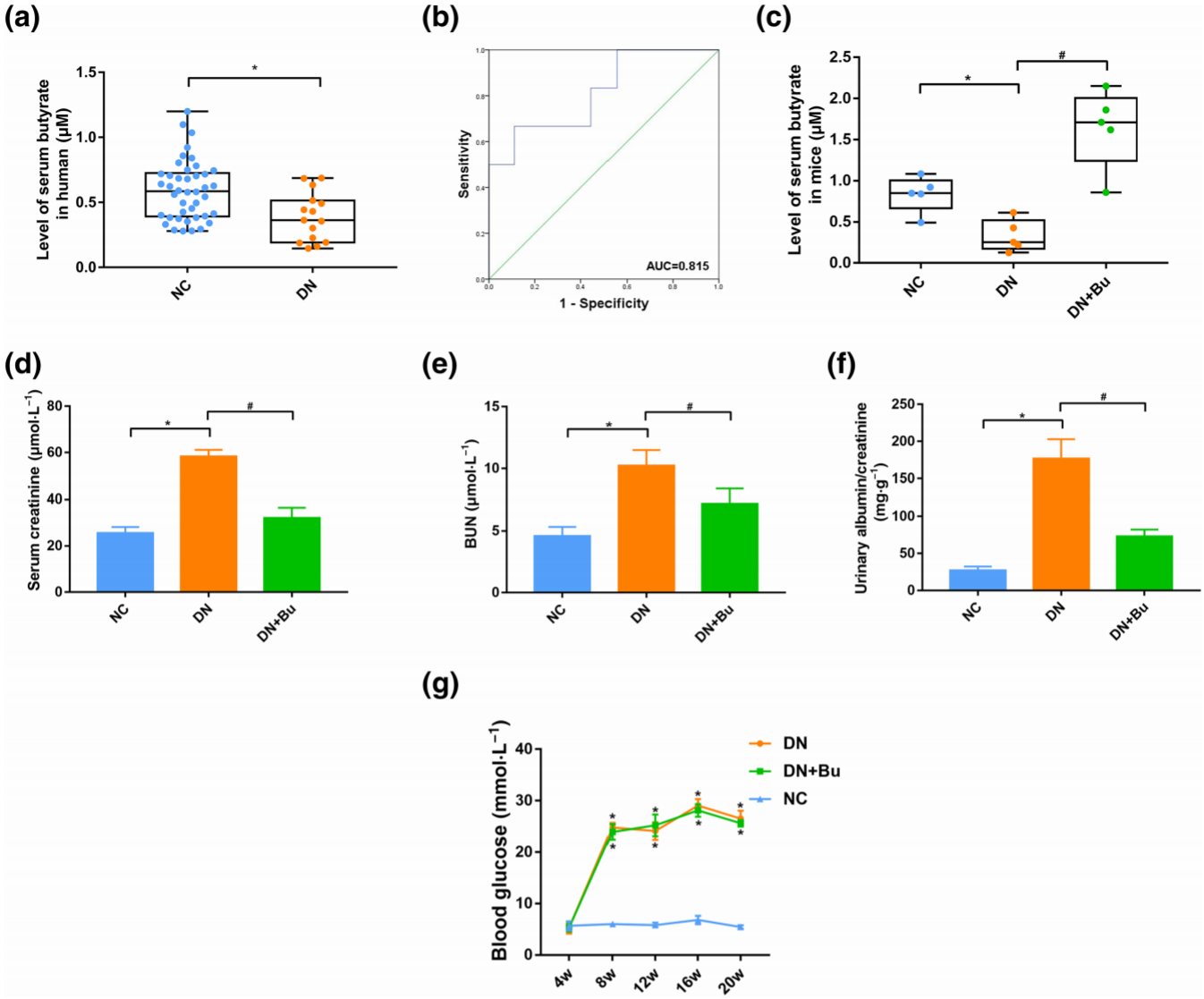

FIGURE 2 Butyrate is significantly correlated with DN and protects renal functions. Butyrate levels were decreased in DN (in-patients, $n = 15$), compared with healthy subjects ($n = 42$) (a). The ROC curve, to evaluate the diagnostic value of muscle atrophy, is shown in (b). Butyrate levels was also measured in db/db mice, with or without butyrate treatment ($n = 5$) (c). Butyrate reduced the levels of serum creatinine, BUN, and urinary albumin/creatinine ratio of db/db mice ($n = 5$) (d–f). Blood glucose of db/db mice exhibited no obvious changes with butyrate treatment ($n = 5$) (g). $^{*}P < 0.05$, significantly different from NC; $^{\#}P < 0.05$, significantly different as indicated

Alcian blue stained all mucins, which were secreted by goblet cells. Muc2 is the most distinctive and prominent mucin secreted in the intestinal tract. Thus, we used immunofluorescence techniques and found that the expression of Muc2 in the ileum and colon was significantly reduced in the db/db mice. Butyrate treatment significantly improved Muc2 levels (Figure 4c,d).

These results indicate that mucins and Muc2 all exhibited significant changes in the ileum and colon. However, the overall expression of mucins and Muc2 in the colon was higher than that in the ileum. Further, We used colon tissues in further analysis of intestinal TJ proteins. Our immunohistochemistry (IHC) data showed that the levels of TJ proteins, ZO-1, and occluding, were significantly lower in db/db mice and butyrate treatment improved them (Figure 4e,f). Immunoblot analysis also suggested that the levels of ZO-1 and occludin of colon in db/db mice were clearly decreased compared with those in the NC group, and butyrate treatment abolished this reduction (Figure 4g).

We then explored the effects of damaging the intestinal barrier on muscle atrophy, in mice with butyrate supplementation (Bu-db/db mice). An alcohol-containing diet (see Supplementary Information) was used to damage the intestinal barrier function of db/db mice (Lu et al., 2017; Summa et al., 2013). The results showed that the levels of mucin, ZO-1, and occludin were significantly reduced after alcohol-containing diet in Bu-db/db mice (Figure S2A,B). Meanwhile, the alcohol-containing diet also decreased the hindlimb mass and cross-sectional area of muscle fibres of Bu-db/db mice (Figure S2C,D). The experiments demonstrated the protective effect of butyrate on muscle atrophy disappeared after damaging intestinal

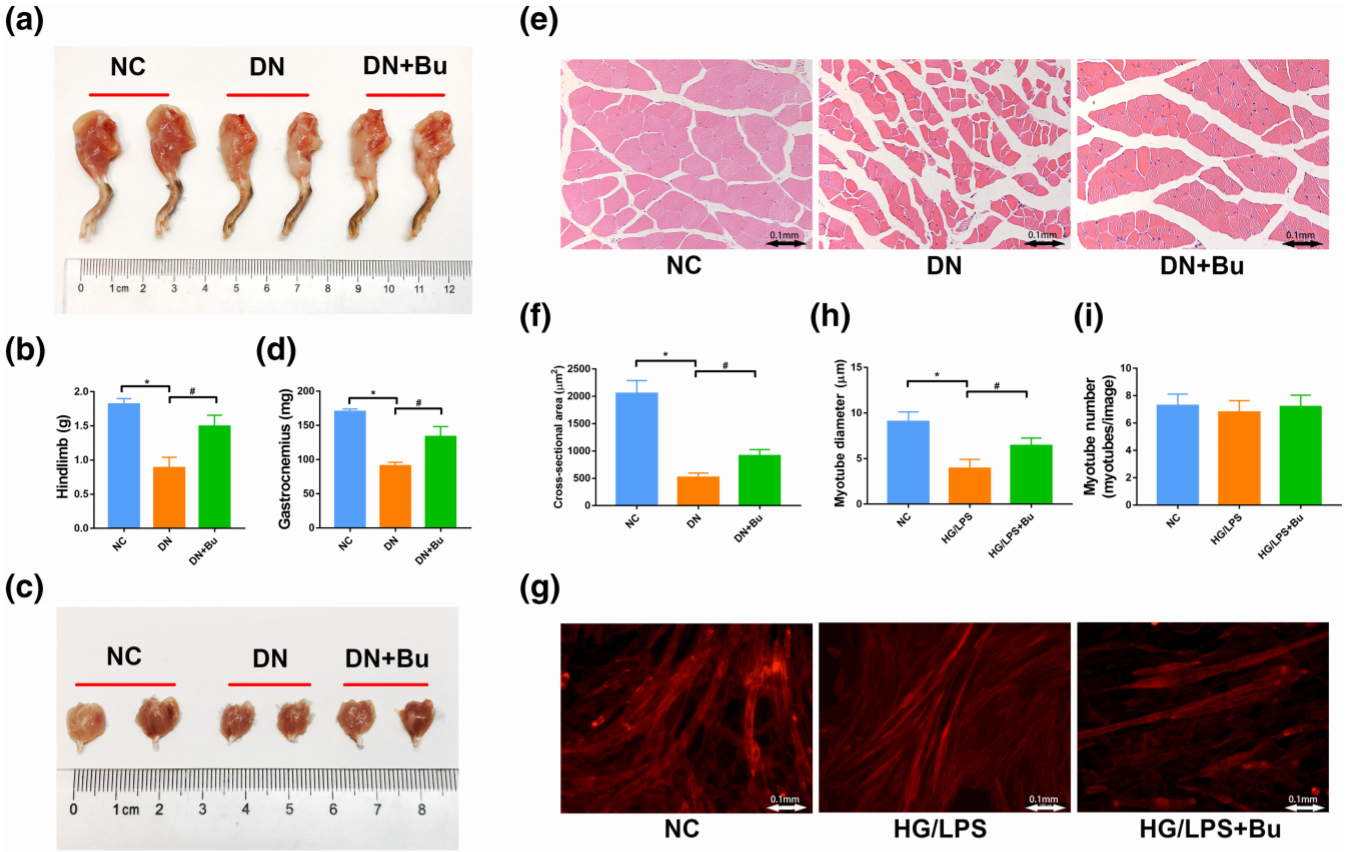

FIGURE 3 Butyrate prevents DN-induced muscle atrophy. The hindlimb (a,b) and gastrocnemius (c,d) muscle masses were quantified and displayed. The volume of transverse muscle fibre was evaluated using H&E staining (e,f). C2C12 myoblasts incubated with HG/LPS for 24 h exhibited an almost 50% reduction in myotube diameter, but there were no changes in myotube numbers (g–i). Data are presented as the mean ± SD with five independent values per group ($n = 5$). $^{*}P < 0.05$, significantly different from NC; $^{\#}P < 0.05$, significantly different as indicated

barrier function by alcohol-containing diet in db/db mice. It indicated that butyrate alleviated DN-induced muscle atrophy by improving the intestinal barrier function.

3.5 | Butyrate suppressed autophagy and oxidative stress, and activated the PI3K/Akt/mTOR pathway in db/db mice and HG/LPS-induced C2C12 myoblasts

Autophagy-lysosomal proteolysis plays an important role in DN-induced muscle atrophy. During autophagy, double membranes form around defective organelles or cytoplasmic proteins that are disrupted or damaged. To evaluate the effect of butyrate on autophagy in muscle atrophy, we observed the formation of autophagosomes and autolysosomes, using transmission electron microscopy (TEM) in mouse skeletal muscle tissue (Figure 5a). The results showed that the number of autophagosomes and autolysosomes in db/db mice was distinctly higher than that in the NC group. After butyrate treatment, the number of autophagosomes and autolysosomes was reduced. To confirm the inhibitory effect of butyrate on autophagy, we used western blotting to measure the expression of LC3II and p62 in skeletal muscle and C2C12 myoblasts. We found that levels of LC3II were significantly increased, while p62 expression was decreased both in skeletal muscle of db/db mice and C2C12 myoblasts incubated with HG/LPS. However, butyrate treatment reversed the up-regulation of LC3II and the down-regulation of p62 (Figure 5b,c).

Previous studies have reported that ROS could induce autophagy. Thus, we examined the influence of butyrate on oxidative stress. Catalase (CAT), glutathione peroxidase (GSH-Px), malondialdehyde (MDA), and superoxide dismutase (SOD) are known biomarkers of the antioxidant defence system and lipid peroxidation. In our studies, we found that the levels of CAT, GSH-Px, and SOD were distinctly decreased in the skeletal muscle of the DN mice, indicating that the antioxidant defence system was impaired in DN (Figure 5d). The damage also occurred in C2C12 myoblasts incubated with HG/LPS, while the ROS activity was increased (Figure 5e,f). However, the effects of the impaired antioxidant defence system was reversed by butyrate treatment, which also alleviated the ROS activity. Correspondingly, both in the skeletal muscle of db/db mice and C2C12 myoblasts incubated with HG/LPS, the levels of MDA were significantly improved, while they were reduced with butyrate treatment (Figure 5d,f).

To further investigate the molecular mechanism underlying butyrate's effect on muscle atrophy, we focused on the oxidative stress-mediated PI3K/Akt/mTOR pathway, the key signalling pathway of

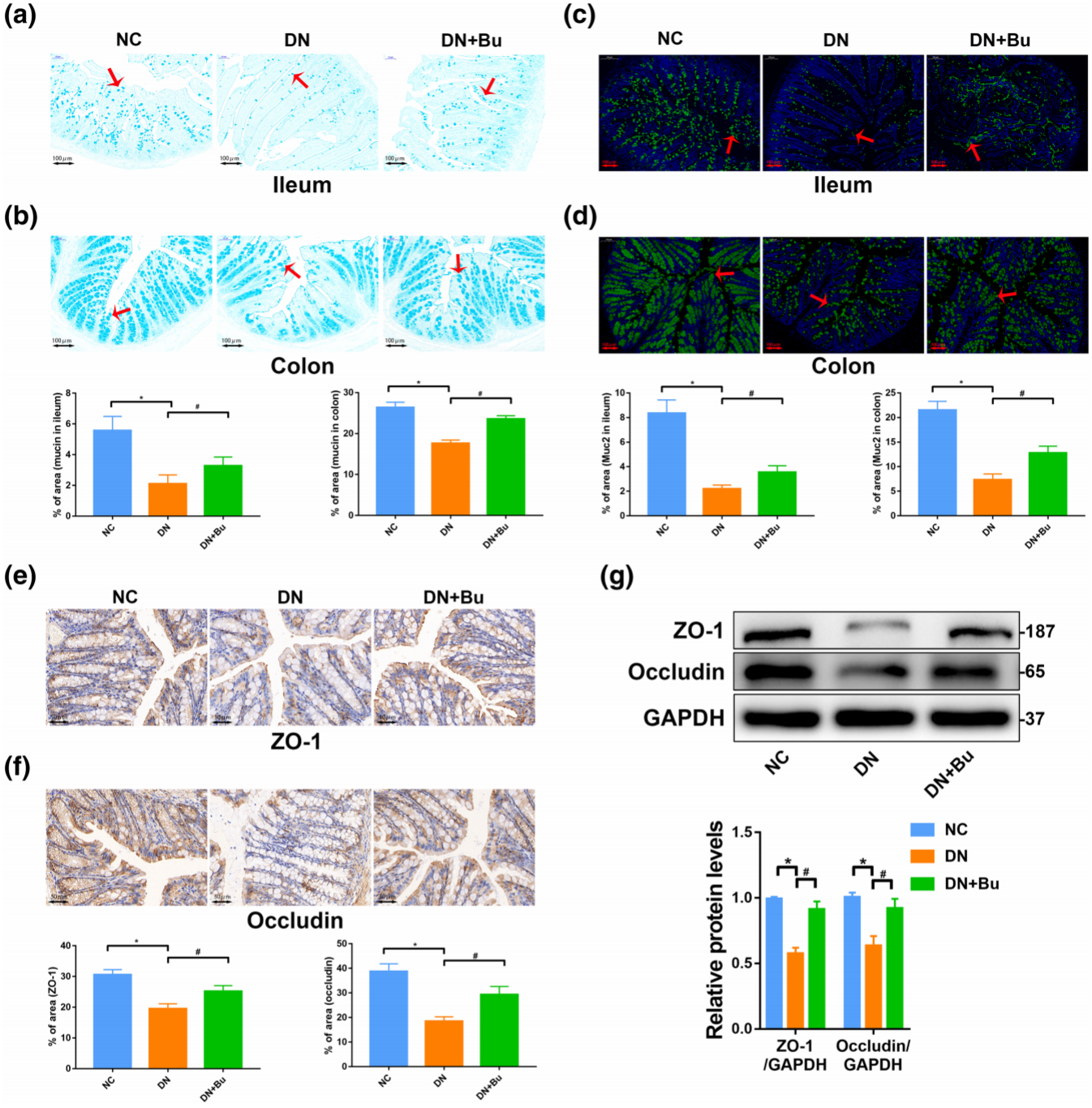

FIGURE 4 Butyrate treatment enhanced the intestinal barrier function in db/db mice. Mucin stained by Alcian blue (shown by the arrows) in ileum and colon is shown (a,b). Muc2 expression in the ileum and colon was analysed using immunofluorescence (shown by the arrows) (c,d). Decreased abundance of colonic ZO-1 and occludin in samples from the db/db mice was reversed by butyrate treatment, as measured by immunohistochemistry (e,f). Representative western blot of ZO-1 and occluding. Levels were significantly reduced in the db/db mice. Butyrate treatment significantly improved ZO-1 and occludin expression (g). Data are presented as the mean ± SD with five independent values per group ($n = 5$). $^{*}P < 0.05$, significantly different from NC; $^{\#}P < 0.05$, significantly different as indicated

protein synthesis. The western blotting results showed that the expression of p-PI3K, p-Akt, and p-mTOR was all significantly decreased in skeletal muscle in the DN group and C2C12 myoblasts exposed to HG/LPS. However, butyrate treatment reversed these changes in both tissues from DN mice and and C2C12 cells (Figure 5g,h).

3.6 | Butyrate inhibited the decrease of FFA2 receptors in db/db mice and HG/LPS-exposed C2C12 myoblasts

Many studies have shown that the FFA2 receptor is a key molecule involved in butyrate-mediated metabolism. However, there is a

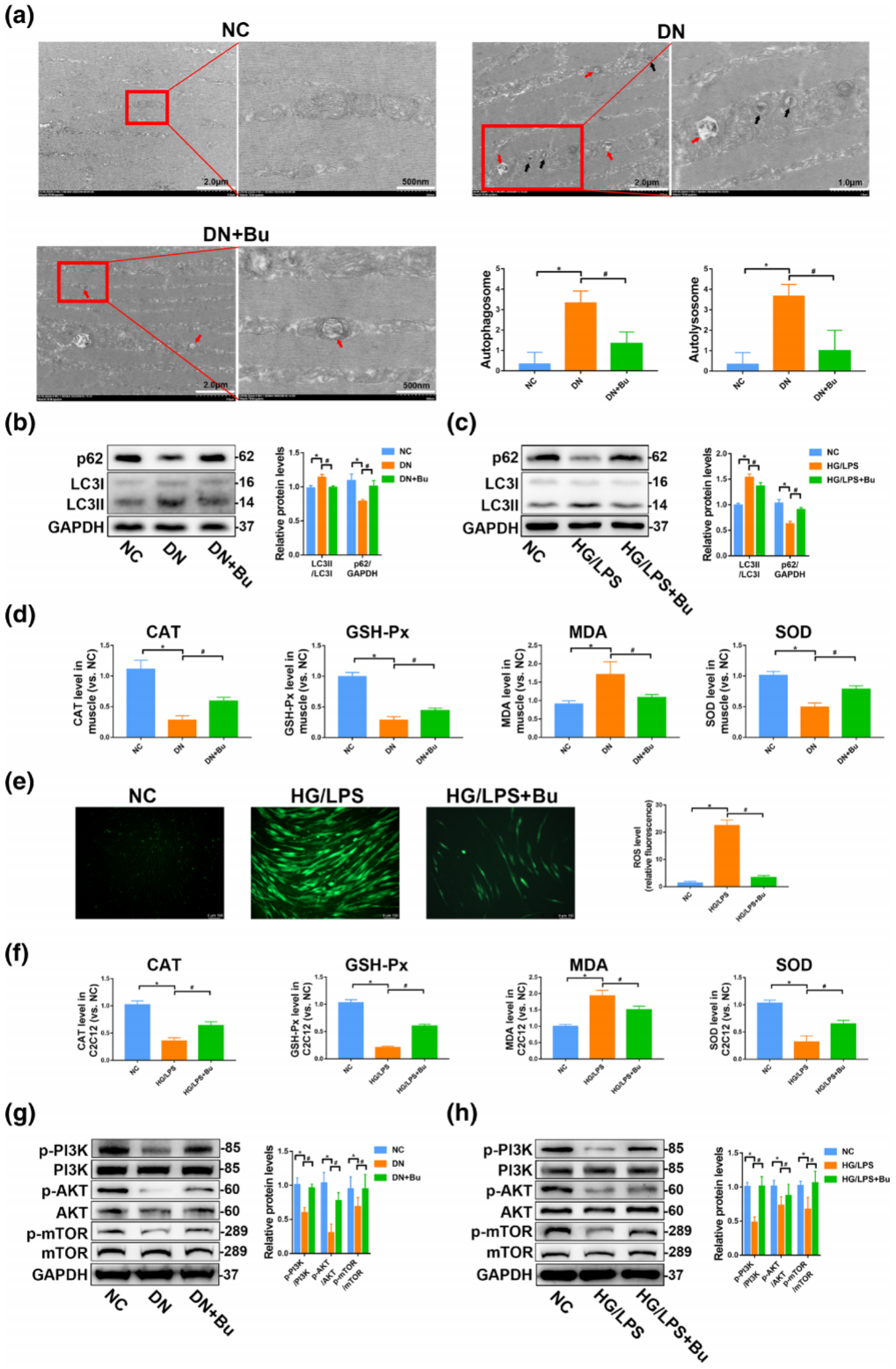

FIGURE 5 Butyrate suppressed autophagy and oxidative stress and activated the PI3K/Akt/mTOR pathway in db/db mice and HG/LPS-induced C2C12 myoblasts. Typical autophagosomes (denoted by black arrows) and autolysosomes (denoted by red arrows) in sections of gastrocnemius were observed under TEM (a). Western blotting analysis indicated LC3II up-regulation and p62 down-regulation in db/db mice (b) and HG/LPS-induced C2C12 myoblasts (c), while the expression of LC3II and p62 followed an opposite trend with butyrate treatment. The activity of CAT, GSH-Px, SOD, and the level of MDA in muscle (d) and serum (f) are shown in the histograms. Intracellular ROS levels were observed using fluorescence microscopy (e). Western blotting results revealed the activation effect of butyrate on p-PI3K, p-Akt and p-mTOR in db/db mice (g) and HG/LPS-induced C2C12 myoblasts (h). Data are presented as the mean ± SD with five independent values per group ($n = 5$). $^{*}P < 0.05$, significantly different from NC; $^{\#}P < 0.05$, significantly different as indicated

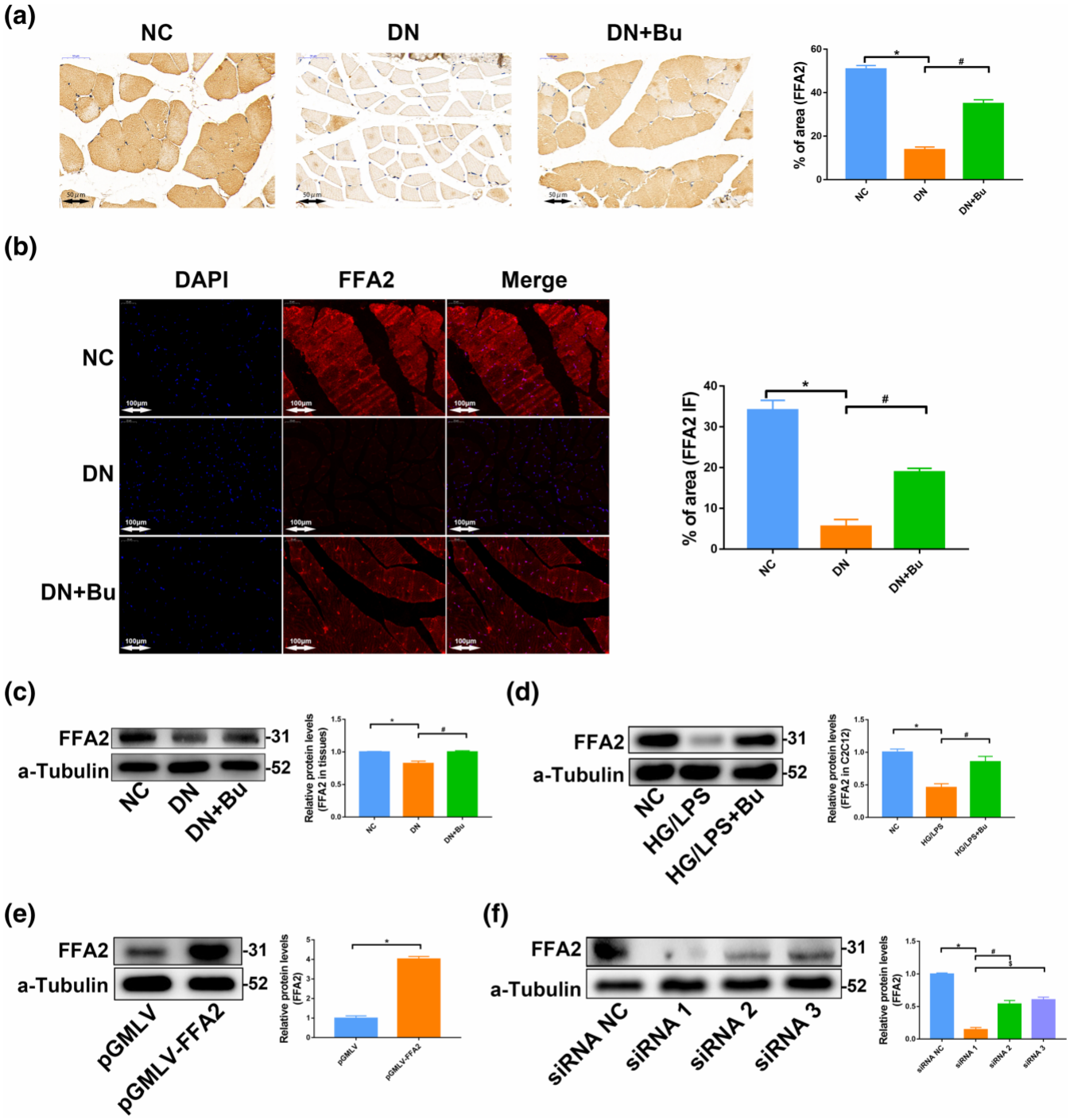

FIGURE 6 Butyrate promotes the up-regulation of FFA2 receptors. Expression of FFA2 protein was assessed in muscle of db/db mice with or without butyrate treatment using immunohistochemistry (a), immunofluorescence (b), and western blotting (c). Levels of FFA2 expression of C2C12 myoblasts were measured in western blots (d). We successfully constructed the stabilized FFA2 overexpression (pGMLV-FFA2) C2C12 myoblasts (e). siRNA 1 (siRNA-FFA2) exerted the best silencing effect on FFA2 (f). Data are presented as the mean ± SD with five independent values per group ($n = 5$). $^{*}P < 0.05$, significantly different from NC, $^{\#}P < 0.05$, $^{\$}P < 0.05$, significantly different as indicated

paucity of information regarding the roles of FFA2 receptors in muscle atrophy. Using IHC and IF, we found that the levels of FFA2 receptors in the skeletal muscle of db/db mice were distinctly decreased, compared with those in the NC group (Figure 6a,b). To obtain further evidence, expression of FFA2 was measured using western blotting. Compared with the NC group, we observed a marked down-regulation of FFA2 in the db/db mice and HG/LPS-induced C2C12 myoblasts (Figure 6c,d). After butyrate treatment, significant up-regulation of FFA2 appeared in all experiments.

To further verify the mechanisms by which FFA2 affects muscle atrophy, we successfully constructed the stabilized, FFA2-overexpressing (pGMLV-FFA2) C2C12 myoblasts and used

these cells with siRNA-mediated gene silencing of FFA2 (Figure 6e,f). We used siRNA 1 (siRNA-FFA2) with the best silencing effect in subsequent experiments.

3.7 | Activation of FFA2 receptors attenuated atrophy by suppressing oxidative stress and autophagy, and activating the PI3K/Akt/mTOR pathway in vivo and in vitro

To confirm the effect of FFA2 receptors on muscle atrophy in vivo, we constructed models of overexpression of FFA2 in db/db mice by TUG-1375 (FFA2 receptor agonist) (Figure S3A) (Hansen et al., 2018). The results showed that the FFA2 receptor agonist significantly increased myofibre cross-sectional area of db/db mice (Figure S3C). The FFA2 receptor agonist also decreased CAT, GSH-Px, and SOD activity and increased MDA (Figure S3E). Compared with the DN group, LC3II expression was distinctly reduced, while p62 expression increased in the DN-TUG group (Figure S3G). Furthermore, the FFA2 receptor agonist improved p-PI3K, p-Akt, and p-mTOR expression ($P < 0.05$; Figure 3I). These results indicated that activation of FFA2 receptors attenuated muscle atrophy by suppressing oxidative stress and autophagy and activating the PI3K/Akt/mTOR pathway in vivo.

The TRITC-phalloidin staining results showed that overexpression of FFA2 reversed the reduction of myotube diameters in HG/LPS-exposed C2C12 myoblasts, while silencing of FFA2 did not improve this decrease (Figure 7a,b). Meanwhile, regardless of whether FFA2 expression changed, the number of myotubes remained unchanged (Figure S4A, B).

To observe the influence of FFA2 receptors on autophagy, we used western blotting to measure the levels of LC3II and p62. Compared with the HG/LPS group, we found that the LC3II expression was distinctly decreased, while p62 expression increased in the pGMLV-FFA2 group (Figure 7c). However, silencing FFA2 prevented it from reversing LC3II up-regulation and p62 down-regulation (Figure 7d).

We analysed ROS levels by examining fluorescence and oxidative stress-related factors, including CAT, GSH-Px, SOD, and MDA in C2C12 myoblasts. Our studies found that overexpression of FFA2 reduced the strong ROS fluorescence, induced by HG/LPS (Figure 7e), whereas the staining intensity did not significantly decrease upon silencing of FFA2, compared with that induced by HG/LPS (Figure 7f). HG/LPS also resulted in decreased CAT, GSH-Px, and SOD activity and increased MDA, which were reversed by overexpression of FFA2, but not by FFA2 silencing (Figure S4C,D).

To evaluate whether the beneficial effect of FFA2 on muscle atrophy was related to the PI3K/Akt/mTOR pathway in C2C12 myoblasts, we measured the levels of p-PI3K, p-Akt, and p-mTOR. Overexpression of FFA2 significantly improved p-PI3K, p-AKT, and p-mTOR expression (Figure 7g). However, the effect disappeared with FFA2 silencing (Figure 7h). This also indicated that FFA2 promoted activation of the PI3K/Akt/mTOR pathway to alleviate muscle atrophy in vitro.

3.8 | Butyrate alleviated muscle atrophy via FFA2 receptors by reducing oxidative stress and activating the PI3K/Akt/mTOR pathway

According to the experiments described above, both overexpression of FFA2 receptors and butyrate treatment attenuated HG/LPS-induced C2C12 myoblast atrophy. To examine whether butyrate attenuated the atrophy through FFA2 receptors, HG/LPS was used to treat pGMLV-FFA2 and siRNA-FFA2 C2C12 myoblasts. After TRITC-phalloidin staining, we observed that the beneficial effect of butyrate against C2C12 myoblast morphological atrophy disappeared in siRNA-FFA2 C2C12 myoblasts, which suggested that butyrate could not alleviate muscle atrophy without expression of FFA2 (Figures 8a and S5A). In addition, increased ROS fluorescence, MDA levels, and decreased CAT, GSH-Px, and SOD activity in HG/LPS-induced siRNA-FFA2 C2C12 myoblasts did not change, with or without butyrate treatment (Figures 8b and S5B–D). Similarly, butyrate significantly suppressed the up-regulation of LC3II and down-regulation of p62 in HG/LPS-induced pGMLV-FFA2 C2C12 myoblasts (Figure S5E), whereas these effects were not reversed in siRNA-FFA2 C2C12 myoblasts (Figure 8c). Further studies showed that the ability of butyrate to activate the PI3K/Akt/mTOR pathway also disappeared in HG/LPS-induced siRNA-FFA2 C2C12 myoblasts (Figures 8d and S5F). We also established lentivirus-mediated muscle FFA2 inhibition in db/db mice with butyrate supplementation (Bu-db/db mice) (Figure S6A). Consistent with the results from our in vitro experiments, the effect of butyrate on inhibiting muscle atrophy via blocking oxidative stress and activating the PI3K/Akt/mTOR pathway also disappeared after inhibition of FFA2 expression (Figure S6B–E). These results indicated that butyrate inhibited the oxidative stress-mediated PI3K/Akt/mTOR pathway in muscle atrophy, possibly by up-regulating expression of FFA2.

4 | DISCUSSION

Butyrate is the least abundant SCFA. Previous studies have demonstrated that it has antioxidant, anti-inflammatory, and immunomodulatory effects, regulates intestinal barrier function, and modulates diabetic-endotoxaemia (Chang et al., 2014; Gao et al., 2009; Gonzalez et al., 2019; Xu et al., 2018). However, there are few reports on the protective effect of butyrate against oxidative damage and fibrosis in DN kidneys (Krokowicz et al., 2014), but no reports of correlations between butyrate and muscle atrophy in DN. In this study, we have quantitated metabolites in serum and found a significant decrease of butyrate in patients with DN and modest accuracy in the diagnosis of muscle atrophy. The db/db mice have a mutation deletion of the leptin receptor and are frequently used as models of Type 2 diabetes (Sun et al., 2018). The underlying genetic background of db/db mice makes them susceptible to obesity and diabetic complications such as nephropathy (Azushima et al., 2018). In our experiments, we demonstrated that loss of renal function and skeletal muscle atrophy can be reversed by adding butyrate to the diet of db/db mice. Further,

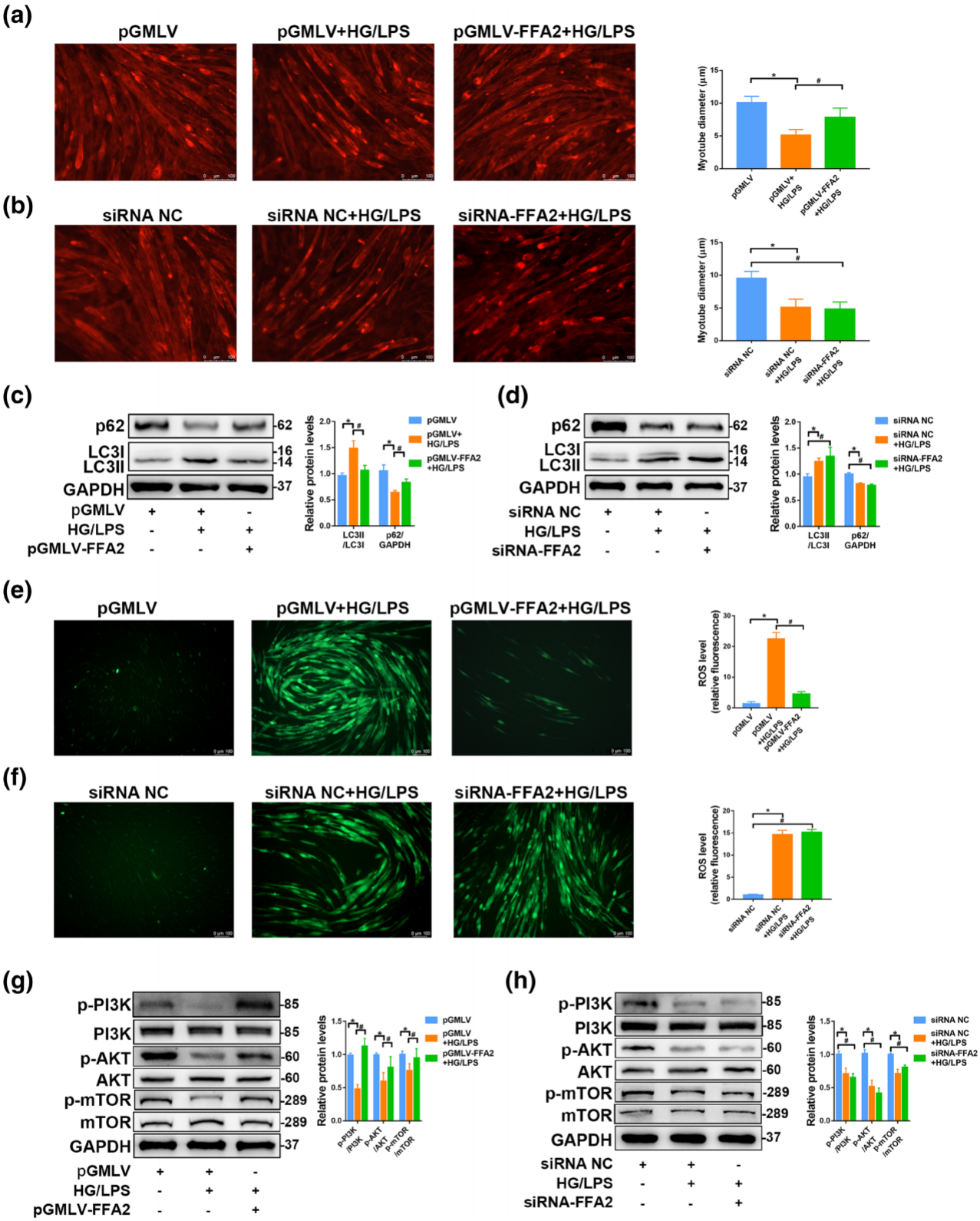

FIGURE 7 FFA2 regulates atrophy via oxidative stress, autophagy and the PI3K/Akt/mTOR pathway. TRITC-phalloidin staining shows morphological atrophy of HG/LPS-induced C2C12 myoblasts with silencing of FFA2 expression, which was reversed by FFA2 overexpression (a,b). Western blotting showed the overexpression of FFA2 also reversed the up-regulation of LC3II and down-regulation of p62 in HG/LPS-induced C2C12 myoblasts, while silencing of FFA2 did not (c,d). Fluorescence (e,f) showed the generation of ROS HG/LPS-induced C2C12 myoblasts. FFA2 overexpression (g) promoted p-PI3K, p-Akt, and p-mTOR in HG/LPS-induced C2C12 myoblasts via Western blotting, but silencing of FFA2 did not (h). Data are presented as the mean ± SD with five independent values per group ($n = 5$). $^{*}P < 0.05$, $^{\#}P < 0.05$, significantly different as indicated

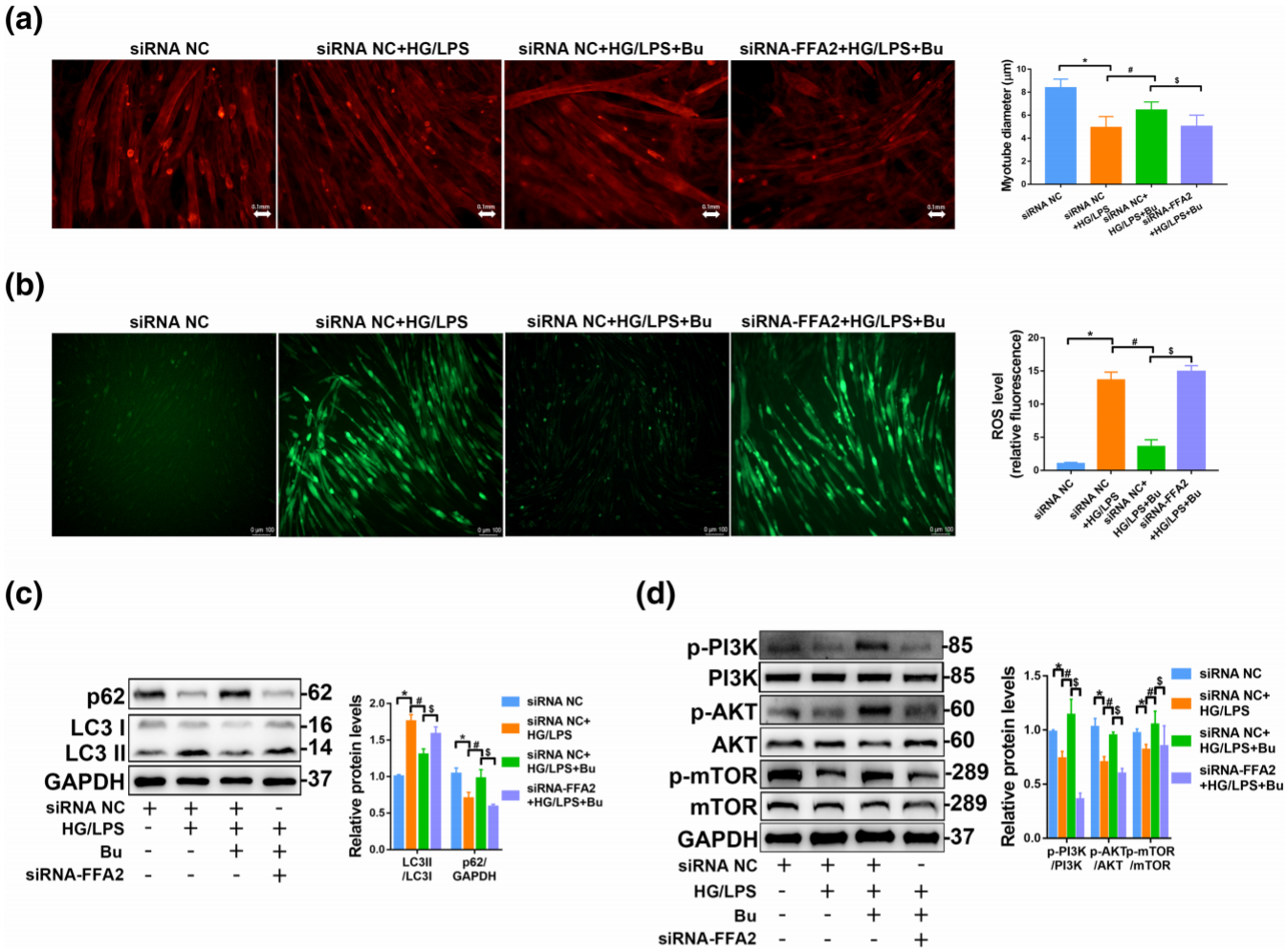

FIGURE 8 Butyrate suppresses muscle atrophy by activating FFA2 receptors, and subsequent oxidative stress, the PI3K/Akt/mTOR pathway, and autophagy. Butyrate no longer inhibited atrophy in HG/LPS-induced C2C12 myoblasts with FFA2 silencing, as shown by TRITC-phalloidin staining (a). Silencing of FFA2 prevented butyrate from decreasing ROS generation (b). Western blotting revealed that LC3II up-regulation and p62 down-regulation in HG/LPS-induced C2C12 myoblasts were not reversed by butyrate in the absence of FFA2 (c). Without FFA2, butyrate could not increase the levels of p-PI3K, p-Akt, and p-mTOR to activate the PI3K/Akt/mTOR pathway (d). Data are presented as the mean ± SD with five independent values per group ($n = 5$). $^{*}P < 0.05$, $^{\#}P < 0.05$, $^{\$}P < 0.05$, significantly different as indicated

inflammatory factors in muscles and serum were also markedly reduced after butyrate treatment in db/db mice. In addition, butyrate significantly decreased the elevation of serum LPS, which was consistent with enhanced intestinal barrier function after butyrate treatment in db/db mice. Increased ROS production and decreased antioxidant enzymes commonly result in oxidative stress, which contributes to DN-induced muscle atrophy. Our present study also confirmed decreased production of ROS and of antioxidant enzyme activity, including CAT, GSH-Px, and SOD, which were reversed after butyrate treatment in db/db mice. Furthermore, we confirmed that these effects involved the PI3K/Akt/mTOR pathway (the key pathway related to protein synthesis), which was activated by butyrate in db/db mice. In addition, we demonstrated that FFA2 receptors were critical in regulating oxidative stress, the PI3K/Akt/mTOR pathway, and autophagy in muscle atrophy of DN, through overexpression or silencing of FFA2.

'Diabetic-endotoxaemia' is a new concept according to the characteristic of low-grade chronic inflammation (elevated inflammatory cytokines and LPS) in Type 2 diabetes (Gomes et al., 2017). As one of the long-term complications of diabetes, DN is a primary cause of end-stage renal disease (Dronavalli et al., 2008). Diabetic-endotoxaemia has also been recognized as a risk factor that is closely associated with both the onset and the progression of Type 2 diabetes and subsequent DN (Dronavalli et al., 2008). Recently, gut dysbacteriosis was shown to contribute to gut-leak, which plays a pivotal role in the source of this endotoxaemia (Denis et al., 2015). Numerous studies have confirmed that increased LPS levels contribute to CKD-induced muscle atrophy, from in vivo or in vitro experiments (Baker et al., 2018; Wang & Mitch, 2014). Thus, we hypothesized and demonstrated that butyrate ameliorated DN-induced muscle atrophy by preserving gut integrity, which suppressed the transposition of LPS from the gut to circulation. Austin et al. found

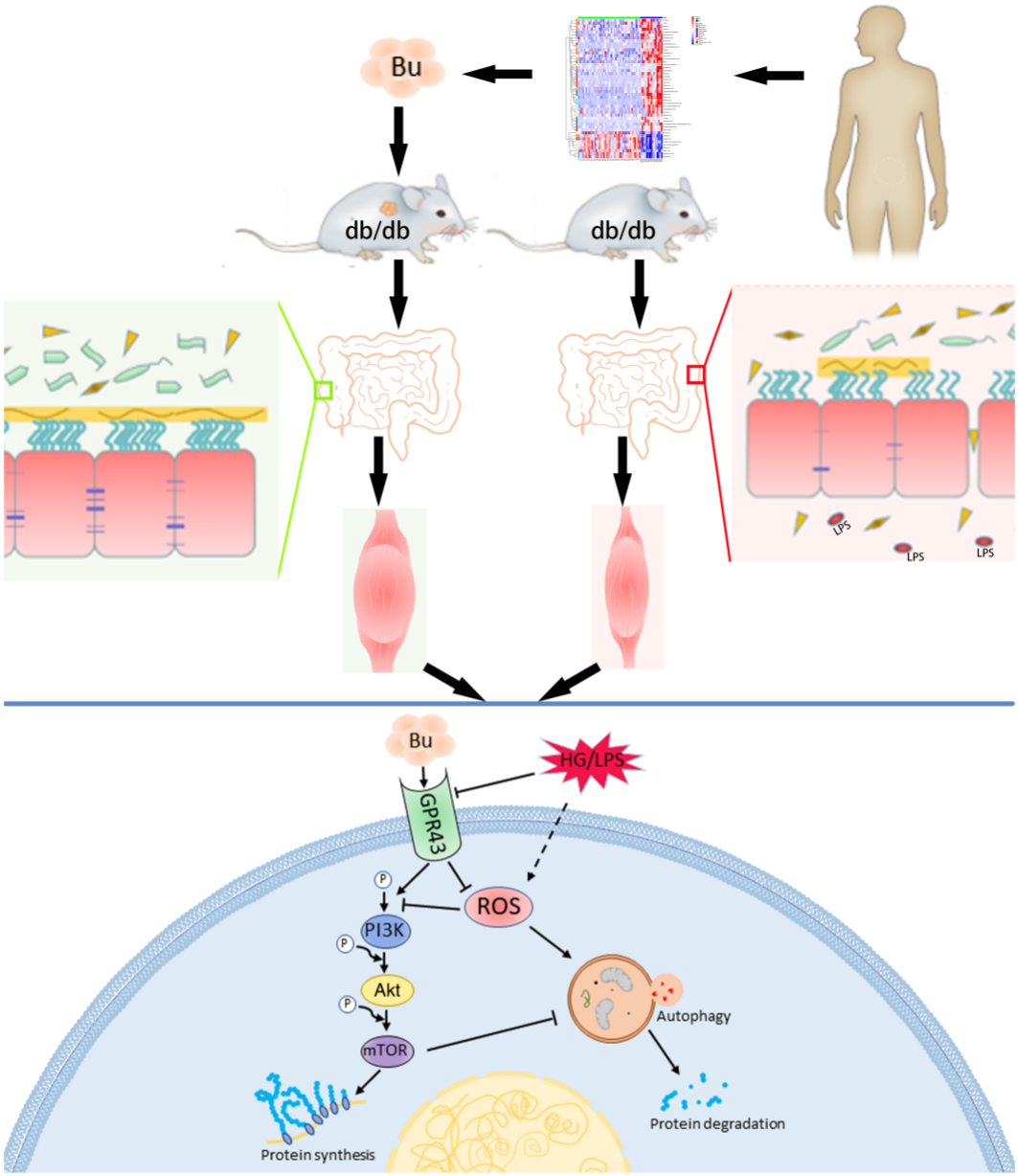

FIGURE 9 Diagram illustrating the processes and mechanisms of this study. GPR43, FFA2 receptor

that butyrate ameliorated renal failure in CKD rats by improving mucin expression (Gonzalez et al., 2019), which was similar to our results in db/db mice. Reduction in serum LPS levels inhibited muscle atrophy. Therefore, our studies demonstrated that butyrate mitigated muscle atrophy by enhancing intestinal barrier function.

Mitochondria are a key source of ROS, which are produced by normal metabolism in the body (Murphy, 2009). Mitochondrial dysfunction (no data provided) and decreased antioxidant enzyme activities result in elevated ROS production, which leads to oxidative stress. Furthermore, oxidative stress contributes to the pathogenesis and development of muscle injury (Ryan et al., 2011), and Wang et al. (2019) showed that ROS production and oxidative stress also contributed to CKD-induced muscle atrophy. Some researchers have observed mitochondrial dysfunction in the skeletal muscle of CKD rats (Enoki et al., 2017). In fact, we also observed morphological swelling in db/db mice. Mitochondrial dysfunction leads to loss of mitochondrial mass and reduces the energy production. Oxidative stress, in turn, damages the mitochondria. Together, these constitute a vicious cycle, producing more ROS-aggravating muscle atrophy. However, ROS play a positive role at low, regulated concentrations under physiological conditions (Di Meo et al., 2016). They participate in the regulation of many cellular processes, including differentiation, proliferation, growth, apoptosis, cytoskeletal regulation, migration, and contraction (Krause, 2007). This delicate balance between appropriate redox states and oxidative stress is disrupted under pathological conditions. Oxidative stress is manifested by increased ROS generation and destruction of many cellular organelles and proteins, which are involved in muscle atrophy. In this study, we

observed the harmful influence of oxidative stress on muscle atrophy in db/db mice.

We also observed increased autophagy and activation of the PI3K/Akt/mTOR pathway in the muscle of db/db mice and in cell models. Although the influence of CKD on the activation of autophagy has not been rigorously evaluated, recent studies have suggested that autophagy plays a role in exacerbating muscle atrophy in CKD (Abrigo et al., 2018; Su et al., 2017). In one study, the rate of proteolysis in isolated muscles decreased when lysosomal functions were inhibited with weak bases (Wang & Mitch, 2014). Studies have shown that autophagy is activated by oxidative stress. However, the mechanisms by which ROS affect DN-induced muscle atrophy by regulating autophagy remain unclear. Importantly, the formation of autophagosomes is stimulated by decreased levels of p-PI3K, and CKD suppresses PI3K/Akt signalling, which also stimulates the autophagy–lysosome system (Sandri, 2013). ROS suppressed or promoted autophagy via activation of Src/PI3K/Akt or inhibition of the Akt/mTOR pathway in different models of muscle atrophy (Pal et al., 2014; Talbert et al., 2013). Therefore, the antioxidant effect of butyrate suggests that it can suppress oxidative stress and consequently inhibit autophagy mediated by the PI3K/Akt/mTOR pathway, to protect against muscle atrophy, induced by DN.

Butyrate acts as an extracellular stimulus in the intracellular activities outlined above, which raises the question about how an extracellular component mediates this intracellular signal transduction. Interestingly, FFA2 receptors are the primary receptor for SCFAs (Tan et al., 2014). These receptors are expressed along the entire gastrointestinal tract, including cells of both the immune and nervous systems (Tan et al., 2014). Recent studies have shown that SCFAs may regulate adipocyte development in adiposity, modulate the development or differentiation of immune cells, and play an anti-inflammatory role (Dewulf et al., 2013; Maslowski et al., 2009; Senga et al., 2003; Voltolini et al., 2012). However, there are no reports regarding FFA2 expression and its regulatory effect on muscle atrophy. Although FFA2 and FFA3 receptors are activated by the same group of SCFAs, there is a distinct rank order of potency that has been established for FFA2 and FFA3 (Hudson et al., 2012). In our experiments, we used western blot to show that levels of FFA3 were not significantly changed in our in vitro or in vivo experiments (Figure S7A,B). Current studies have also shown SCFAs (acetate, propionate, and butyrate) had no significantly different potency and all were able to stimulate FFA2 receptors in DN mice (Huang et al., 2020). Besides, we performed enrichment analysis for potential pathway and found the butyrate metabolism pathway was the most valuable metabolism pathway for further assessments (Figure 1c). Therefore, we hypothesized that butyrate reverses DN-induced muscle atrophy by regulating FFA2. First, we demonstrated that expression of FFA2 in muscle in db/db mice was significantly lower than those in the NC group. Furthermore, our study showed that butyrate treatment improved hindlimb and gastrocnemius mass in db/db mice, which was confirmed by FFA2 receptor-mediated activation of the PI3K/Akt/mTOR pathway, which was crucial to the up-regulation of autophagy induced by oxidative stress.. Therefore, FFA2, as the specific receptor of SCFAs, could be more useful in promoting butyrate to treat DN-induced muscle atrophy. However, the strict molecular mechanism needs further research.

In conclusion, our analysis of the metabolomics showed butyrate to be the key metabolite (Figure 9). We demonstrated the beneficial effects of butyrate on intestinal barrier function and muscle atrophy in db/db mice and HG/LPS-induced C2C12 myoblasts. We were able to show that butyrate ameliorated DN-induced muscle atrophy by stimulation and up-regulation of FFA2 receptors. This effect was mainly achieved by the PI3K/Akt/mTOR pathway, which regulates the oxidative stress-mediated autophagy in DN-induced muscle atrophy. Our studies suggest that butyrate may be clinically useful as a novel drug to protect against muscle atrophy by enhancing intestinal barrier function and promoting FFA2 receptor-mediated PI3K/Akt/mTOR pathway in DN.

ACKNOWLEDGEMENTS

The authors thank Dr Jing Han from Department of Orthopaedics, Shanghai General Hospital and Dr Bin Li from Department of gastroenterology, Shanghai General Hospital for providing assistance. This study was supported by the National Natural Science Foundation of China (grant nos. 81700621 and 81970624).

AUTHOR CONTRIBUTIONS

G.T., S.R., and W.J.Y. conceived and designed the study. G.T., Y.D., and H.C.G. carried out the acquisition, analysis, and interpretation of data. G.T., Y.D., H.C.G., J.S.J., N.Z., and Y.P.S wrote the manuscript. S.R. and W.J.Y. supervised the study.

CONFLICT OF INTEREST

The authors declare that there is no conflict of interest regarding the publication of this paper.

DECLARATION OF TRANSPARENCY AND SCIENTIFIC RIGOUR

This Declaration acknowledges that this paper adheres to the principles for transparent reporting and scientific rigour of preclinical research as stated in the *BJP* guidelines for Design and Analysis, Immunoblotting and Immunochemistry, and Animal Experimentation, and as recommended by funding agencies, publishers, and other organizations engaged with supporting research.

DATA AVAILABILITY STATEMENT

The data that support the findings of this study are available from the corresponding author upon reasonable request.

REFERENCES

Abrigo, J., Elorza, A. A., Riedel, C. A., Vilos, C., Simon, F., Cabrera, D., Estrada, L., & Cabello-Verrugio, C. (2018). Role of oxidative stress as key regulator of muscle wasting during cachexia. *Oxidative Medicine and Cellular Longevity*, *2018*, 1–17. https://doi.org/10.1155/2018/2063179

Alexander, S. P., Christopoulos, A., Davenport, A. P., Kelly, E., Mathie, A., Peters, J. A., Veale, E. L., Armstrong, J. F., Faccenda, E., Harding, S. D., Pawson, A. J., Southan, C., Davies, J. A., Abbracchio, M. P.,

Alexander, W., Al-hosaini, K., Bäck, M., Barnes, N. M., Bathgate, R., … Ye, R. D. (2021). The Concise Guide to PHARMACOLOGY 2021/22: G protein-coupled receptors. *British Journal of Pharmacology*, *178*(S1), S27–S156. https://doi.org/10.1111/bph.15538

Alexander, S. P., Fabbro, D., Kelly, E., Mathie, A., Peters, J. A., Veale, E. L., Armstrong, J. F., Faccenda, E., Harding, S. D., Pawson, A. J., Southan, C., Davies, J. A., Beuve, A., Brouckaert, P., Bryant, C., Burnett, J. C., Farndale, R. W., Friebe, A., Garthwaite, J., … Waldman, S. A. (2021a). The Concise Guide to PHARMACOLOGY 2021/22: Catalytic receptors. *British Journal of Pharmacology*, *178*(S1), S264–S312. https://doi.org/10.1111/bph.15541

Alexander, S. P., Fabbro, D., Kelly, E., Mathie, A., Peters, J. A., Veale, E. L., Armstrong, J. F., Faccenda, E., Harding, S. D., Pawson, A. J., Southan, C., Davies, J. A., Boison, D., Burns, K. E., Dessauer, C., Gertsch, J., Helsby, N. A., Izzo, A. A., Koesling, D., … Wong, S. S. (2021b). The Concise Guide to PHARMACOLOGY 2021/22: Enzymes. *British Journal of Pharmacology*, *178*(S1), S313–S411. https://doi.org/10.1111/bph.15542

Anders, H. J., Andersen, K., & Stecher, B. (2013). The intestinal microbiota, a leaky gut, and abnormal immunity in kidney disease. *Kidney International*, *83*(6), 1010–1016. https://doi.org/10.1038/ki.2012.440

Andrade-Oliveira, V., Amano, M. T., Correa-Costa, M., Castoldi, A., Felizardo, R. J., de Almeida, D. C., Bassi, E. J., Moraes-Vieira, P. M., Hiyane, M. I., Rodas, A. C., & Peron, J. P. (2015). Gut bacteria products prevent AKI induced by ischemia-reperfusion. *J Am Soc Nephrol*, *26*(8), 1877–1888. https://doi.org/10.1681/ASN.2014030288

Azushima, K., Gurley, S. B., & Coffman, T. M. (2018). Modelling diabetic nephropathy in mice. *Nature Reviews. Nephrology*, *14*(1), 48–56. https://doi.org/10.1038/nrneph.2017.142

Baker, L. A., Martin, N. R. W., Kimber, M. C., Pritchard, G. J., Lindley, M. R., & Lewis, M. P. (2018). Resolvin E1 (R_VE_1) attenuates LPS induced inflammation and subsequent atrophy in C2C12 myotubes. *Journal of Cellular Biochemistry*, *119*(7), 6094–6103. https://doi.org/10.1002/jcb.26807

Chang, P. V., Hao, L., Offermanns, S., & Medzhitov, R. (2014). The microbial metabolite butyrate regulates intestinal macrophage function via histone deacetylase inhibition. *Proceedings of the National Academy of Sciences of the United States of America*, *111*(6), 2247–2252. https://doi.org/10.1073/pnas.1322269111

Cheng, D., Xu, J. H., Li, J. Y., Wang, S. Y., Wu, T. F., Chen, Q. K., & Yu, T. (2018). Butyrate ameliorated-NLRC3 protects the intestinal barrier in a GPR43-dependent manner. *Experimental Cell Research*, *368*(1), 101–110. https://doi.org/10.1016/j.yexcr.2018.04.018

Denis, M. C., Desjardins, Y., Furtos, A., Marcil, V., Dudonne, S., Montoudis, A., Garofalo, C., Delvin, E., Marette, A., & Levy, E. (2015). Prevention of oxidative stress, inflammation and mitochondrial dysfunction in the intestine by different cranberry phenolic fractions. *Clinical Science (London, England)*, *128*(3), 197–212. https://doi.org/10.1042/CS20140210

Dewulf, E. M., Ge, Q., Bindels, L. B., Sohet, F. M., Cani, P. D., Brichard, S. M., & Delzenne, N. M. (2013). Evaluation of the relationship between gpr43 and adiposity in human. *Nutrition & Metabolism (London)*, *10*(1), 11. https://doi.org/10.1186/1743-7075-10-11

Di Meo, S., Reed, T. T., Venditti, P., & Victor, V. M. (2016). Role of ROS and RNS sources in physiological and pathological conditions. *Oxidative Medicine and Cellular Longevity*, *2016*, 1–44. https://doi.org/10.1155/2016/1245049

Dong, W., Jia, Y., Liu, X., Zhang, H., Li, T., Huang, W., Chen, X., Wang, F., Sun, W., & Wu, H. (2017). Sodium butyrate activates NRF2 to ameliorate diabetic nephropathy possibly via inhibition of HDAC. *The Journal of Endocrinology*, *232*(1), 71–83. https://doi.org/10.1530/JOE-16-0322

Dronavalli, S., Duka, I., & Bakris, G. L. (2008). The pathogenesis of diabetic nephropathy. *Nature Clinical Practice. Endocrinology & Metabolism*, *4*(8), 444–452. https://doi.org/10.1038/ncpendmet0894

Du, Y., Yang, Y. T., Tang, G., Jia, J. S., Zhu, N., & Yuan, W. J. (2020). Butyrate alleviates diabetic kidney disease by mediating the miR-7a-5p/P311/TGF-β1 pathway. *The FASEB Journal*, *34*, 10462–10475. https://doi.org/10.1096/fj.202000431R

Enoki, Y., Watanabe, H., Arake, R., Fujimura, R., Ishiodori, K., Imafuku, T., Nishida, K., Sugimoto, R., Nagao, S., Miyamura, S., Ishima, Y., Tanaka, M., Matsushita, K., Komaba, H., Fukagawa, M., Otagiri, M., & Maruyama, T. (2017). Potential therapeutic interventions for chronic kidney disease-associated sarcopenia via indoxyl sulfate-induced mitochondrial dysfunction. *Journal of Cachexia, Sarcopenia and Muscle*, *8*(5), 735–747. https://doi.org/10.1002/jcsm.12202

Fouque, D., Kalantar-Zadeh, K., Kopple, J., Cano, N., Chauveau, P., Cuppari, L., Franch, H., Guarnieri, G., Ikizler, T. A., Kaysen, G., Lindholm, B., Massy, Z., Mitch, W., Pineda, E., Stenvinkel, P., Trevinho-Becerra, A., & Wanner, C. (2008). A proposed nomenclature and diagnostic criteria for protein-energy wasting in acute and chronic kidney disease. *Kidney International*, *73*(4), 391–398. https://doi.org/10.1038/sj.ki.5002585

Franke, T. F., Hornik, C. P., Segev, L., Shostak, G. A., & Sugimoto, C. (2003). PI3K/Akt and apoptosis: Size matters. *Oncogene*, *22*(56), 8983–8998. https://doi.org/10.1038/sj.onc.1207115

Gao, Z., Yin, J., Zhang, J., Ward, R. E., Martin, R. J., Lefevre, M., Cefalu, W. T., & Ye, J. (2009). Butyrate improves insulin sensitivity and increases energy expenditure in mice. *Diabetes*, *58*(7), 1509–1517. https://doi.org/10.2337/db08-1637

Glick, D., Barth, S., & Macleod, K. F. (2010). Autophagy: Cellular and molecular mechanisms. *The Journal of Pathology*, *221*(1), 3–12. https://doi.org/10.1002/path.2697

Gomes, J. M. G., Costa, J. A., & Alfenas, R. C. G. (2017). Metabolic endotoxemia and diabetes mellitus: A systematic review. *Metabolism*, *68*, 133–144. https://doi.org/10.1016/j.metabol.2016.12.009

Gonzalez, A., Krieg, R., Massey, H. D., Carl, D., Ghosh, S., Gehr, T. W. B., & Ghosh, S. S. (2019). Sodium butyrate ameliorates insulin resistance and renal failure in CKD rats by modulating intestinal permeability and mucin expression. *Nephrology, Dialysis, Transplantation*, *34*(5), 783–794. https://doi.org/10.1093/ndt/gfy238

Haneda, M., Utsunomiya, K., Koya, D., Babazono, T., Moriya, T., Makino, H., Kimura, K., Suzuki, Y., Wada, T., Ogawa, S., Inaba, M., Kanno, Y., Shigematsu, T., Masakane, I., Tsuchiya, K., Honda, K., Ichikawa, K., & Shide, K. (2015). A new classification of diabetic nephropathy 2014: A report from joint committee on diabetic nephropathy. *Clinical and Experimental Nephrology*, *19*(1), 1–5. https://doi.org/10.1007/s10157-014-1057-z

Hanna, R. M., Ghobry, L., Wassef, O., Rhee, C. M., & Kalantar-Zadeh, K. (2020). A practical approach to nutrition, protein-energy wasting, sarcopenia, and cachexia in patients with chronic kidney disease. *Blood Purification*, *49*(1–2), 202–211. https://doi.org/10.1159/000504240

Hansen, A. H., Sergeev, E., Bolognini, D., Sprenger, R. R., Ekberg, J. H., Ejsing, C. S., McKenzie, C. J., Rexen Ulven, E., Milligan, G., & Ulven, T. (2018). Discovery of a potent thiazolidine free fatty acid receptor 2 agonist with favorable pharmacokinetic properties. *Journal of Medicinal Chemistry*, *61*(21), 9534–9550. https://doi.org/10.1021/acs.jmedchem.8b00855

Huang, W., Man, Y., Gao, C., Zhou, L., Gu, J., Xu, H., Wan, Q., Long, Y., Chai, L., Xu, Y., & Xu, Y. (2020). Short-chain fatty acids ameliorate diabetic nephropathy via GPR43-mediated inhibition of oxidative stress and NF-κb signaling. *Oxidative Medicine and Cellular Longevity*, *2020*, 1–21. https://doi.org/10.1155/2020/4074832

Hudson, B. D., Tikhonova, I. G., Pandey, S. K., Ulven, T., & Milligan, G. (2012). Extracellular ionic locks determine variation in constitutive activity and ligand potency between species orthologs of the free fatty acid receptors FFA2 and FFA3. *The Journal of Biological Chemistry*, *287*(49), 41195–41209. https://doi.org/10.1074/jbc.M112.396259

Kameyama, A., Dong, W., & Matsuno, Y. K. (2015). Succinylation-Alcian blue staining of mucins on polyvinylidene difluoride membranes.

Methods in Molecular Biology, *1314*, 325–331. https://doi.org/10.1007/978-1-4939-2718-0_33

Katso, R., Okkenhaug, K., Ahmadi, K., White, S., Timms, J., & Waterfield, M. D. (2001). Cellular function of phosphoinositide 3-kinases: Implications for development, homeostasis, and cancer. *Annual Review of Cell and Developmental Biology*, *17*, 615–675. https://doi.org/10.1146/annurev.cellbio.17.1.615

Kim, K. W., Baek, M. O., Choi, J. Y., Son, K. H., & Yoon, M. S. (2019). Analysis of the molecular signaling signatures of muscle protein wasting between the intercostal muscles and the gastrocnemius muscles in db/db mice. *International Journal of Molecular Sciences*, *20*(23), 6062. https://doi.org/10.3390/ijms20236062

Krause, K. H. (2007). Aging: A revisited theory based on free radicals generated by NOX family NADPH oxidases. *Experimental Gerontology*, *42*(4), 256–262. https://doi.org/10.1016/j.exger.2006.10.011

Krokowicz, L., Stojcev, Z., Kaczmarek, B. F., Kociemba, W., Kaczmarek, E., Walkowiak, J., Krokowicz, P., Drews, M., & Banasiewicz, T. (2014). Microencapsulated sodium butyrate administered to patients with diverticulosis decreases incidence of diverticulitis—A prospective randomized study. *International Journal of Colorectal Disease*, *29*(3), 387–393. https://doi.org/10.1007/s00384-013-1807-5

Li, Y. J., Chen, X., Kwan, T. K., Loh, Y. W., Singer, J., Liu, Y., Ma, J., Tan, J., Macia, L., Mackay, C. R., Chadban, S. J., & Wu, H. (2020). Dietary fiber protects against diabetic nephropathy through short-chain fatty acid-mediated activation of G protein-coupled receptors GPR43 and GPR109a. *Journal of the American Society of Nephrology*, *31*(6), 1267–1281. https://doi.org/10.1681/ASN.2019101029

Lilley, E., Stanford, S. C., Kendall, D. E., Alexander, S. P. H., Cirino, G., Docherty, J. R., George, C. H., Insel, P. A., Izzo, A. A., Ji, Y., Panettieri, R. A., Sobey, C. G., Stefanska, B., Stephens, G., Teixeira, M., & Ahluwalia, A. (2020). ARRIVE 2.0 and the British Journal of Pharmacology: Updated guidance for 2020. *British Journal of Pharmacology*, *177*(16), 3611–3616. https://doi.org/10.1111/bph.15178

Lu, R., Voigt, R. M., Zhang, Y., Kato, I., Xia, Y., Forsyth, C. B., Keshavarzian, A., & Sun, J. (2017). Alcohol injury damages intestinal stem cells. *Alcoholism, Clinical and Experimental Research*, *41*(4), 727–734. https://doi.org/10.1111/acer.13351

Maslowski, K. M., Vieira, A. T., Ng, A., Kranich, J., Sierro, F., Yu, D., Schilter, H. C., Rolph, M. S., Mackay, F., Artis, D., & Xavier, R. J. (2009). Regulation of inflammatory responses by gut microbiota and chemoattractant receptor GPR43. *Nature*, *461*(7268), 1282–1286. https://doi.org/10.1038/nature08530

Milligan, G., Stoddart, L. A., & Smith, N. J. (2009). Agonism and allosterism: The pharmacology of the free fatty acid receptors FFA2 and FFA3. *British Journal of Pharmacology*, *158*(1), 146–153. https://doi.org/10.1111/j.1476-5381.2009.00421.x

Murphy, M. P. (2009). How mitochondria produce reactive oxygen species. *The Biochemical Journal*, *417*(1), 1–13. https://doi.org/10.1042/BJ20081386

Nallu, A., Sharma, S., Ramezani, A., Muralidharan, J., & Raj, D. (2017). Gut microbiome in chronic kidney disease: Challenges and opportunities. *Translational Research*, *179*, 24–37. https://doi.org/10.1016/j.trsl.2016.04.007

Obi, Y., Qader, H., Kovesdy, C. P., & Kalantar-Zadeh, K. (2015). Latest consensus and update on protein-energy wasting in chronic kidney disease. *Current Opinion in Clinical Nutrition and Metabolic Care*, *18*(3), 254–262. https://doi.org/10.1097/MCO.0000000000000171

Pal, R., Palmieri, M., Loehr, J. A., Li, S., Abo-Zahrah, R., Monroe, T. O., Thakur, P. B., Sardiello, M., & Rodney, G. G. (2014). Src-dependent impairment of autophagy by oxidative stress in a mouse model of Duchenne muscular dystrophy. *Nature Communications*, *5*, 4425. https://doi.org/10.1038/ncomms5425

Percie du Sert, N., Hurst, V., Ahluwalia, A., Alam, S., Avey, M. T., Baker, M., Browne, W. J., Clark, A., Cuthill, I. C., Dirnagl, U., & Emerson, M. (2020). The ARRIVE guidelines 2.0: Updated guidelines for reporting animal research. *PLoS Biology*, *18*(7), e3000410. https://doi.org/10.1371/journal.pbio.3000410

Ryan, M. J., Jackson, J. R., Hao, Y., Leonard, S. S., & Alway, S. E. (2011). Inhibition of xanthine oxidase reduces oxidative stress and improves skeletal muscle function in response to electrically stimulated isometric contractions in aged mice. *Free Radical Biology & Medicine*, *51*(1), 38–52. https://doi.org/10.1016/j.freeradbiomed.2011.04.002

Sandri, M. (2013). Protein breakdown in muscle wasting: Role of autophagy-lysosome and ubiquitin-proteasome. *The International Journal of Biochemistry & Cell Biology*, *45*(10), 2121–2129. https://doi.org/10.1016/j.biocel.2013.04.023

Senga, T., Iwamoto, S., Yoshida, T., Yokota, T., Adachi, K., Azuma, E., Hamaguchi, M., & Iwamoto, T. (2003). LSSIG is a novel murine leukocyte-specific GPCR that is induced by the activation of STAT3. *Blood*, *101*(3), 1185–1187. https://doi.org/10.1182/blood-2002-06-1881

Su, Z., Klein, J. D., Du, J., Franch, H. A., Zhang, L., Hassounah, F., Hudson, M. B., & Wang, X. H. (2017). Chronic kidney disease induces autophagy leading to dysfunction of mitochondria in skeletal muscle. *American Journal of Physiology. Renal Physiology*, *312*(6), F1128–F1140. https://doi.org/10.1152/ajprenal.00600.2016

Summa, K. C., Voigt, R. M., Forsyth, C. B., Shaikh, M., Cavanaugh, K., Tang, Y., Vitaterna, M. H., Song, S., Turek, F. W., & Keshavarzian, A. (2013). Disruption of the circadian clock in mice increases intestinal permeability and promotes alcohol-induced hepatic pathology and inflammation. *PLoS ONE*, *8*(6), e67102. https://doi.org/10.1371/journal.pone.0067102

Sun, S. F., Tang, P. M. K., Feng, M., Xiao, J., Huang, X. R., Li, P., Ma, R. C. W., & Lan, H. Y. (2018). Novel lncRNA Erbb4-IR promotes diabetic kidney injury in db/db mice by targeting miR-29b. *Diabetes*, *67*(4), 731–744. https://doi.org/10.2337/db17-0816

Talbert, E. E., Smuder, A. J., Min, K., Kwon, O. S., Szeto, H. H., & Powers, S. K. (2013). Immobilization-induced activation of key proteolytic systems in skeletal muscles is prevented by a mitochondria-targeted antioxidant. *Journal of Applied Physiology (Bethesda, MD: 1985)*, *115*(4), 529–538. https://doi.org/10.1152/japplphysiol.00471.2013

Tan, J., McKenzie, C., Potamitis, M., Thorburn, A. N., Mackay, C. R., & Macia, L. (2014). The role of short-chain fatty acids in health and disease. *Advances in Immunology*, *121*, 91–119. https://doi.org/10.1016/B978-0-12-800100-4.00003-9

Vaziri, N. D., Wong, J., Pahl, M., Piceno, Y. M., Yuan, J., DeSantis, T. Z., Ni, Z., Nguyen, T. H., & Andersen, G. L. (2013). Chronic kidney disease alters intestinal microbial flora. *Kidney International*, *83*(2), 308–315. https://doi.org/10.1038/ki.2012.345

Vaziri, N. D., Yuan, J., Rahimi, A., Ni, Z., Said, H., & Subramanian, V. S. (2012). Disintegration of colonic epithelial tight junction in uremia: A likely cause of CKD-associated inflammation. *Nephrology, Dialysis, Transplantation*, *27*(7), 2686–2693. https://doi.org/10.1093/ndt/gfr624

Vaziri, N. D., Zhao, Y. Y., & Pahl, M. V. (2016). Altered intestinal microbial flora and impaired epithelial barrier structure and function in CKD: The nature, mechanisms, consequences and potential treatment. *Nephrology, Dialysis, Transplantation*, *31*(5), 737–746. https://doi.org/10.1093/ndt/gfv095

Voltolini, C., Battersby, S., Etherington, S. L., Petraglia, F., Norman, J. E., & Jabbour, H. N. (2012). A novel antiinflammatory role for the short-chain fatty acids in human labor. *Endocrinology*, *153*(1), 395–403. https://doi.org/10.1210/en.2011-1457

Wang, M., Hu, R., Wang, Y., Liu, L., You, H., Zhang, J., Wu, X., Pei, T., Wang, F., Lu, L., Xiao, W., & Wei, L. (2019). Atractylenolide III attenuates muscle wasting in chronic kidney disease via the oxidative stress-mediated PI3K/AKT/mTOR pathway. *Oxidative Medicine and Cellular Longevity*, *2019*, 1–16. https://doi.org/10.1155/2019/1875471

Wang, X. H., Du, J., Klein, J. D., Bailey, J. L., & Mitch, W. E. (2009). Exercise ameliorates chronic kidney disease-induced defects in muscle protein metabolism and progenitor cell function. *Kidney International*, *76*(7), 751–759. https://doi.org/10.1038/ki.2009.260

Wang, X. H., & Mitch, W. E. (2014). Mechanisms of muscle wasting in chronic kidney disease. *Nature Reviews. Nephrology*, *10*(9), 504–516. https://doi.org/10.1038/nrneph.2014.112

Xu, Y. H., Gao, C. L., Guo, H. L., Zhang, W. Q., Huang, W., Tang, S. S., Gan, W. J., Xu, Y., Zhou, H., & Zhu, Q. (2018). Sodium butyrate supplementation ameliorates diabetic inflammation in db/db mice. *The Journal of Endocrinology*, *238*(3), 231–244. https://doi.org/10.1530/JOE-18-0137

Zhang, W. Q., Zhao, T. T., Gui, D. K., Gao, C. L., Gu, J. L., Gan, W. J., Huang, W., Xu, Y., Zhou, H., Chen, W. N., Liu, Z. L., & Xu, Y. H. (2019). Sodium butyrate improves liver glycogen metabolism in type 2 diabetes mellitus. *Journal of Agricultural and Food Chemistry*, *67*(27), 7694–7705. https://doi.org/10.1021/acs.jafc.9b02083

SUPPORTING INFORMATION

Additional supporting information may be found in the online version of the article at the publisher's website.

How to cite this article: Tang, G., Du, Y., Guan, H., Jia, J., Zhu, N., Shi, Y., Rong, S., & Yuan, W. (2022). Butyrate ameliorates skeletal muscle atrophy in diabetic nephropathy by enhancing gut barrier function and FFA2-mediated PI3K/Akt/mTOR signals. *British Journal of Pharmacology*, *179*(1), 159–178. https://doi.org/10.1111/bph.15693